Heliyon 10 (2024) e37505

Contents lists available at ScienceDirect

Heliyon

journal homepage: www.cell.com/heliyon

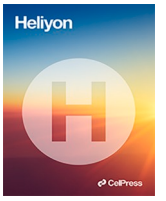

Research article

Comprehensive analysis of the electronic, thermodynamic, and spectroscopic properties of a Cu(II)-based complex with 1,10-phenanthroline and L-glutamine

Marinaldo V. Souza Junior [a], João G. Oliveira Neto [a], Walajhone O. Pereira [a], Jéssica A.O. Rodrigues [a], Jailton R. Viana [a], Aramys S. Reis [a], Mateus R. Lage [a,b], Guilherme G.C. Carvalho [c], Cláudia O. Pessoa [c], Adenilson O. dos Santos [a], Francisco F. de Sousa [a,d,*]

[a] *Center for Sciences of Imperatriz, Health and Technology, Federal University of Maranhão - UFMA, 65900-410, Imperatriz, MA, Brazil*
[b] *Coordination of the Science and Technology Course, Federal University of Maranhão – UFMA, 65800-000, Balsas, MA, Brazil*
[c] *Experimental Oncology Laboratory, Nucleus for Research in Drug Development (NPDM), Fortaleza, CE, 60430-270, Brazil*
[d] *Institute of Exact and Natural Sciences, Federal University of Pará-UFPA, 66075-110, Belém, PA, Brazil*

ARTICLE INFO

Keywords:
Copper complex
Physical and chemical characterizations
DFT studies
Solvation effects
Cytotoxic activity

ABSTRACT

This study reports additional information's of geometric, electronic, thermodynamic, and vibrational properties of a Cu(II) complex with 1,10-phenanthroline and L-glutamine ligands. The experimental spectroscopic analyses were corroborated by density functional theory (DFT). Furthermore, these properties were evaluated using an implicit solvation method with water and methanol solvents, including vacuum condition. The theoretical predictions provided a deeper understanding of the frontier molecular orbitals, chemical reactivity indices, dipole moment, and electrostatic potential maps. A computational analysis of the intermolecular interactions using Hirshfeld surfaces was also performed, which demonstrated that the H···O/O···H and H···H interactions are mainly responsible for the structural and thermal stability of the complex. The calculated intramolecular vibration bands showed a good correlation with the experimental Raman and infrared (IR) data, although solvation effects caused some wavenumber shifts. *In vitro*, antitumor assays were performed to evaluate the cytotoxic effects of the complex against prostate (PC-3) and glioblastoma (SNB-19) cancer cells. Absorption, distribution, metabolism, and excretion (ADME) parameters, along with drug-like properties, are also presented in this work.

1. Introduction

Copper(II)-based coordination compounds have recently aroused attention of the scientific community. This interest stems from their potential biological activities when complexed with heterocyclic molecules, such as 1,10-phenanthroline (phen) and amino acids [1–5]. These activities encompass a range of properties, including antibacterial, antineoplastic, antacid, antifungal, anti-inflammatory, and antiviral properties [1,2,4,5]. Furthermore, the geometric nature of Cu(II) metal center depends on the ligands' structure and may affect physicochemical properties, solubility, redox action, structural variability, and coordination number [6,7].

* Corresponding author. Institute of Exact and Natural Sciences, Federal University of Pará-UFPA, 66075-110, Belém, PA, Brazil.
E-mail address: ffs@ufpa.br (F.F. Sousa).

https://doi.org/10.1016/j.heliyon.2024.e37505
Received 28 March 2024; Received in revised form 3 September 2024; Accepted 4 September 2024
Available online 5 September 2024

Cu(II) allows us to obtain stable complexes with various ligands, including amino acids [8–12]. This ability supplies several applications, as pointed out by Corona-Motolinia et al. [13], in which the interaction of metal-amino acid complexes in biological systems was analyzed. In addition, the formation of Cu(II)-based ternary complexes can modify the physicochemical properties of amino acids, making them more reactive and it can alter their three-dimensional structures [14,15]. However, almost no studies exist on the electronic, vibrational, thermal, and chemical properties of coordination compounds, including theoretical predictions via density functional theory (DFT) calculations [16–19]. Such studies have primarily focused on experiments of structure determination and a limited number of cytotoxicity assays.

Another important aspect is the transformative effect of Cu(II) presence in the coordination structure of metal-organic complexes. Such inclusion can induce significant alterations in their physicochemical properties, such as chemical reactivity and physical parameters. In fact, it directly modulates thermodynamic factors and quantum descriptors [18–20], which are intrinsically associated with structure-function relationships on the biological properties of Cu(II)-based complexes [15].

Cu(II) has a low cost when applied in cancer therapies in comparison to those metal ions, such as ruthenium (Ru), osmium (Os), rhodium (Rh), and platinum (Pt), which are widely utilized in anticancer complexes [21]. Thus, these characteristics make Cu(II) a promising candidate for applying coordination compounds targeting biological activities. The Cu(II) ion is a biologically active metal, presenting hydrolytic and redox activities upon interacting with specific organic molecules [15,22]. Furthermore, it serves as an essential cofactor in numerous enzymatic processes crucial for the proper functioning of human organisms, including metabolic and breathing processes [23]. Additionally, this metal is abundantly found in several living organisms and, when coordinated by some biomolecules, it can exhibit a cytotoxic effect promoting cell death [24,25].

Some satisfactory and promising results of Cu(II)-based complexes with amino acids have been reported; they are named as [Cu(amino acid)(phen)]H_2O_n. Valora et al. [11] investigated Cu(II) complexes containing phen as main ligand and amino acids as secondary ligands in aqueous solution to determine if the coordination geometry in the solid state is maintained. UV–Vis–NIR spectroscopy, electron paramagnetic resonance (EPR), and formal reduction potentials were used to obtain information on the characteristics and chemical behavior of the complexes in aqueous solution. On the other hand, Madden et al. [12] also studied ternary systems formed by Cu(II), phen, and amino acids in aqueous solution using electromotive force measurements. The data were analyzed with LETAGROP program to obtain species distribution diagrams as a function of pH. Wojciechowska et al. [26] have reported the synthesis of [CuCl(L-arginine)(phen)]Cl·2H_2O complex and its assignment of theoretical IR- and Raman-vibration modes obtained from DFT calculations. The authors also calculated chemical reactivity descriptors using frontier molecular orbitals and surface electrostatic potential for this complex. Although some theoretical-experimental studies highlighting solvent effects on the chemical and biological properties of coordination compounds are reported in the literature [18], there is a noticeable gap in theoretical insights concerning complexes based on bivalent transition metals [27].

Oliveira Neto et al. [1] have recently performed structural, vibrational, and electronic properties studies about [CuCl(glycine)(phen)]3H_2O complex, combined with cytotoxicity against HCT-116 abnormal cells (human colorectal cancer). The authors also verified a good concordance between experimental and theoretical data. Rodrigues et al. [2] have reported that the [Cu(L-methionine)(phen)(H_2O)]Cl·1.5H_2O and [CuCl(L-asparagine)(phen)(H_2O)]H_2O complexes demonstrated high antineoplastic potential against prostate cancer cells (DU-145 and PC-3), breast cancer (MDA-MB-231 and MCF-7), and melanoma (MV3). Additionally, Kiraz et al. [28] have published the synthesis, solved structure, and an antiproliferative assay on Caco-2, A549, MCF-7, and BEAS-2B cells from the [Cu(glutaminato)(phen)(H_2O)]NO_3·H_2O complex, nominate for this study of [Cu(Gln)(phen)(H_2O)]NO_3·H_2O. However, some physicochemical properties, such as study of IR and Raman vibrational bands involving solvation effects, *in silico* pharmacokinetic analysis, intramolecular analysis by Hirshfeld surfaces, thermal analysis, and biological of the Cu(II) complex with phen and L-glutamine (Gln) ligands have not yet been reported.

This work is a review of the data partially described by Kiraz et al. [28], where we sought to clarify the electronic, thermodynamic, and spectroscopic properties' studies of the Cu(II)-complex with phen and Gln, named as [Cu(Gln)(phen)(H_2O)]NO_3·H_2O (the CIF file can be accessed from CSD under the code 1884245 or FODVOM). An experimental investigation of its vibrational properties using Fourier-transform infrared (FT-IR) and Raman spectroscopy is provided. The spectroscopic data were juxtaposed with theoretical data, which were obtained from DFT calculations, also considering solvation effects, through which the vibrational spectra were obtained using the integral equation formalism variant of polarizable continuum model (IEFPCM).

Our theoretical studies also encompass the determination of key molecular orbitals and electrostatic potential maps of [Cu(Gln)(phen)(H_2O)]$^+$ complex. In addition, we employed computational methodologies to elucidate the intermolecular interactions established in the crystalline complex via analysis of Hirsfeld surfaces. Lastly, we assessed the selective cytotoxicity of title complex against prostate (PC-3) and glioblastoma (SNB-19) cancer cells and then complemented these biological assays with a computational method evaluating the absorption, distribution, metabolism, and excretion (ADME) properties along with drug-likeness.

2. Experimental and theoretical methods

2.1. Preparation of crystalline complex

[Cu(Gln)(phen)(H_2O)]NO_3·H_2O crystalline complex was grown from a saturated solution via solvent slow evaporation using 0.5 *m*mol of the following reagents 1,10-phenanthroline (Sigma Aldrich, purity 99 %), Cu(NO_3)$_2$ (Sigma Aldrich, purity ≥99.9 %), Gln (Sigma Aldrich, purity ≥99.9 %) and NaOH (Sigma Aldrich, purity ≥98 %), Then, all reagents were added at a solution of methanol (20 *m*L) and water (5 *m*L). This solution (pH 4.3) was magnetically stirred at 360 RPM for 180 min and, after was filtered. Then, the resulting solution was stored at a controlled temperature (35 °C) until we achieve adequate crystallization. After a period of one a

week, blue crystals have grown with prism-like morphology. This synthesis procedure was followed according to the Kiraz et al. [28].

2.2. Characterization techniques

The crystalline phase of [Cu(Gln)(phen)(H_2O)]NO_3·H_2O crystals were characterized through powder X-ray diffraction (PXRD) using a PANalytical diffractometer (Empyrean) emitting the $K_{\alpha1}$ radiation of Cooper ($\lambda = 1.5418$ Å), operating with 40 kV/40 mA. PXRD was measured in the angular range of $2\theta = 5–50^\circ$ with a step of 0.02° and a counting time of 2 s/step. In addition, Rietveld's method was applied to the experimental pattern using *EXPGUI-GSAS* program [29] from previously published structural data [28].

Thermal measurements were performed simultaneously via thermogravimetry (TG) and differential thermal analysis (DTA) in a Shimadzu DTG-60 analyzer. Thermal measurements of powder sample (~5.16 mg) were obtained in the 303–1173 K temperature interval under N_2 atmosphere with a 100 mL/min flow rate. In addition, differential scanning calorimetry (DSC) measurement was recorded with a Shimadzu DSC-60 equipment. For this analysis, ~2.10 mg of the powder sample was used, with a heating rate of 5 K/min was used under inert nitrogen atmosphere with 100 mL/min flow rate, in the 300–500 K temperature interval.

FT-IR spectroscopy under room-temperature condition was performed with a Vertex 70 V spectrophotometer (Bruker) using KBr pastille method, in the spectral range 400–4000 cm^{-1}. The spectral resolution was 5 cm^{-1}, with an average of 32 scans.

Raman spectrum measurements under room-temperature condition were performed in the 40–3200 cm^{-1} region using a LabRAM spectrometer coupled to a thermoelectric-cooled charge-coupled device (CCD) based on a Peltier-cooled system. The powdered sample was excited with a red solid-state (He-Ne) light source, wave-length 633 nm and power around 3.5 mW. A spectral resolution of 4 cm^{-1} was used. The laser was focused using an Olympus model BX41 microscope.

Molecular absorption spectroscopy in the ultraviolet (UV), visible (Vis) and near-infrared (N-IR) regions were carried out with a Thermo Scientific (Evolution model) spectrophotometer. The experimental setup has a deuterium lamp (double beam) and cuvette of quartz, with an optical path of 0.1 cm. The spectra were measured in the wavelength region of 200–1100 nm. A quantity of 20 mg of the Cu(II)-complex crystals were dissolved in 2 mL of water and methanol; thus, two solutions were prepared from each solvent to record the UV–vis absorption spectra.

2.3. Computational techniques

DFT calculations were developed on the theoretical study of the $[Cu(Gln)(phen)(H_2O)]^+$ complex using the Gaussian 16 computational package [30]. From the XRD structural data [28], the geometry optimization was performed applying the PBE1PBE exchange-correlation functional [31], which has been successfully employed in theoretical calculations of coordination complexes, as reported [2,32]. Furthermore, the 6–311++G(d,p) basis set was applied on C, O, H, and N atoms; while basis functions for valence electrons and Stuttgart-Dresden pseudopotential of the SDD basis set were applied on the Cu atom [33,34].

The first calculations were developed in a vacuum. Additional calculations were carried out accounting for solvation effects using the integral equation formalism of polarizable continuum model (IEFPCM) [35], with the solvents water (1.85 D) and methanol (1.70 D) as dielectric mediums. The theoretical IR and Raman vibrational spectra were obtained and compared to the experimental ones. Further analyses were developed with the vibAnalysis software [36], implemented with a basis on the Bayesian regression method, applying the vibrational mode automatic relevance determination (VMARD) for the study of vibration modes [37]. The predicted Raman and IR modes were corrected using a scale factor of 0.9594 [38]. Then, optimized geometries obtained from the DFT calculations was used to evaluate the *in silico* pharmacokinetic features of the $[Cu(Gln)(phen)(H_2O)]^+$ complex. Therefore, ADME parameters and drug-likeness were estimated using the SwissADME platform [39].

Hirshfeld surfaces [40], fingerprint plots [41,42], and crystal voids were calculated using CrystalExplorer 17 program [43] for the $[Cu(Gln)(phen)(H_2O)]^+$ cationic complex, including the nitrate- and water-free molecules to understand better the intermolecular interactions between all chemical species in the crystal lattice. This study was performed starting from the structure available in Cambridge Structural Database (CSD) under code 1884245. The graphs of Hirshfeld surfaces were obtained according to the normalized distance (d_{norm}), considering the distances from a given point to the nearest external (d_e), internal (d_i) atom, and van der Waals radius (r_{vdW}). The fingerprint plots were obtained in respect to d_e and d_i distances, which provide a description of the intermolecular contacts and allow a quantification of specific interactions [44].

2.4. Cytotoxic assays

To evaluate the cytotoxic effects of the [Cu(Gln)(phen)(H_2O)]NO_3·H_2O complex were used the human tumor cell lines PC-3 (prostate cancer) and SNB-19 (glioblastoma) (both at 3×10^5 cells/ml in 200 µl/well), and the non-tumor murine cell line RAW-264.7 (murine macrophages) (5×10^4 cells/ml in 200 µl/well). The cells were cultured in 96-well plates containing Roswell Park Memorial Institute (RPMI)-1640 medium supplemented with 10 % fetal bovine serum, 2 mM of Gln, 100 U/mL of penicillin, and 100 µg/mL of streptomycin under temperature of 310 K with 5 % CO_2. Following 24 h of incubation, the cells were treated with the [Cu(Gln)(phen)(H_2O)]NO_3·H_2O complex at concentrations ranging from 12.5 to 0.2 µM for an additional 72 h 310 K and 5 % CO_2. For positive control, cisplatin [$PtCl_2(NH_3)_2$] (Sigma Aldrich, purity >99.9 %) was used at concentrations from 50.0 to 0.4 M. Cytotoxicity was evaluated utilizing the 3-(4,5-dimethyl-2-thiazolyl)-2,5-diphenyl-2H-tetrazolium bromide (MTT) assay. After incubation, the medium was replaced with 150 µL of fresh medium with MTT dye (0.5 mg/mL) added. After 3 h, the plates were centrifuged, the formazan was dissolved in 150 µL of DMSO, and absorbance was read at 550 nm. Nonlinear regression analysis was used to determine the mean inhibitory concentration (IC_{50}) and its 95 % confidence intervals (95 % CI). The selectivity index (SI) was then calculated

using this equation:

$$SI = \frac{IC_{50}^{RAW-264.7}}{IC_{50}^{TumorCells}}$$

A selectivity index (SI) greater than 1 means the compounds are more selective for tumor cells than healthy cells *in vitro* [46].

3. Results and discussion

3.1. PXRD and Rietveld's refinement

Fig. 1a shows the PXRD pattern and Rietveld's refinement of $[Cu(Gln)(phen)(H_2O)]NO_3{\cdot}H_2O$ crystals at room-temperature condition. The compound forms crystals in triclinic system, adopting the $P\bar{1}$ (C_i^1) space group, and includes two formula units per unit cell ($Z = 2$). The Rietveld refinement yielded the following unit cell parameters: $a = 7.040(9)$ Å, $b = 12.312(2)$ Å, $c = 12.899(2)$ Å, $\alpha = 110.512(7)°$, $\beta = 105.037(7)°$, $\gamma = 97.373(7)°$, and $V = 981.21(9)$ Å^3. The accuracy of these parameters is indicated by $R_{wp} = 4.7$ %, $R_p = 3.7$ %, and $S = 1.18$, demonstrating that the structural analysis aligns well with previously reported crystallographic data for the $[Cu(Gln)(phen)(H_2O)]NO_3{\cdot}H_2O$ crystal [28].

The asymmetric unit of $[Cu(Gln)(phen)(H_2O)]NO_3{\cdot}H_2O$ coordination complex [28] is displayed in Fig. 1b. As one can note, the bonding atoms (N and O) around copper form a distorted square-pyramidal geometry, due to a spherical impediment that occurs when Gln binds to the transition metal already complexed with phen unit. In the unit cell (Fig. 1c), the molecules are linked across an equatorial plane containing the two organic compounds (phen and Gln) and one H_2O molecule in the axial position. In addition, there are NO_3^- and H_2O molecules in free form, which are established by weaker intermolecular interactions in the crystal lattice, which contribute to the system stability [26], though (the CIF file can be accessed from CSD using code 1884245).

A crystallographic structure similar to $[Cu(Gln)(phen)(H_2O)]NO_3{\cdot}H_2O$ complex is reported in the literature [47], $[Cu(L\text{-glutamine})(phen)(H_2O)]Cl{\cdot}1.5H_2O$ (the CIF file can be accessed from CSD under the code 272495). In this reported complex, the Cu^{2+} ion is coordinated in an equatorial plane by both molecules (Gln and phen), with an H_2O molecule occupying the axial position. Both complexes exhibit a distorted square-pyramidal geometry around the copper ion. However, structural differences are observed between the complex of this work and the complex previously reported [47], such as uncoordinated molecules, symmetry, space group, unit cell parameters, and molecular weight.

3.2. Structure optimization and electronic studies via quantum chemical calculations

The optimized geometries of $[Cu(Gln)(phen)(H_2O)]^+$ complex considering the vacuum, aqueous, and methanolic conditions were obtained using PBE1PBE functional, resulting in a distorted square pyramidal geometry, as presented in Fig. S1 of supplementary material. A better depiction of the structural changes resulting from solvation effects is illustrated in Fig. S2 (supplementary material), where an overlap of the rod-modified structures under varying conditions is presented. DFT calculations were performed only on the coordination complex, that is, the non-coordinated NO_3^- ions and H_2O molecules also present in the crystal were not considered in the calculations, since we focused on understanding the behavior of phen and Gln ligands coordinated to the Cu(II) ion in chemical reactivity indices, which influences biological properties of the complex [4,5]. Each optimized geometry obtained was confirmed as a true minimum in the potential energy surface because all the vibrational frequencies calculated in our theoretical study are positive.

A more detailed analysis of the bond angles and dihedral angles, as well as bond lengths of the $[Cu(Gln)(phen)(H_2O)]^+$ complex

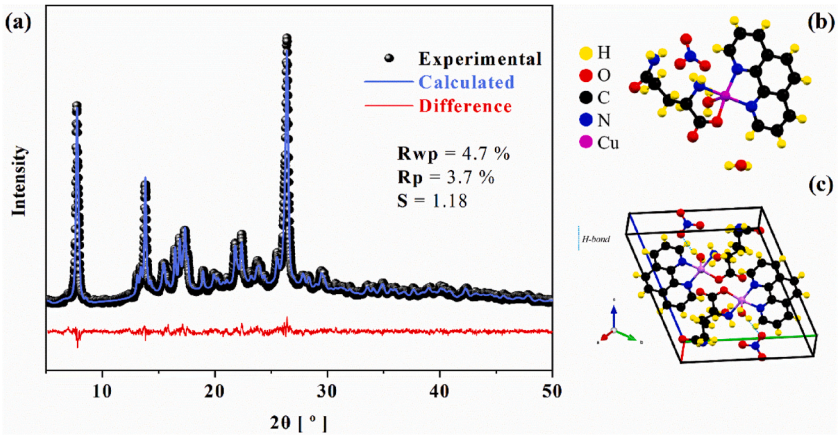

Fig. 1. (a) PXRD Rietveld's refinement for the powdered $[Cu(Gln)(phen)(H_2O)]NO_3{\cdot}H_2O$ crystals at room-temperature condition, (b) molecular structure of complex, and (c) unit cell of monoclinic system in the *bc* plane showing some intermolecular interactions formed between coordination complex and H_2O and NO_3^- molecules.

under different conditions, is provided herein. A comparison between experimental [28] and theoretical data obtained with PB1PBE functional is given in Table S1 (supplementary material). Thus, it is possible to notice in the vacuum-calculated data that even without considering intermolecular interactions occurring in the crystal lattice in the calculations, a good estimate was achieved for almost all structural parameters predicted.

The computed Gibbs free energy of complexation in methanol is −186.25 kcal/mol. The computed Gibbs free energy of complexation in water is −178.36 kcal/mol, indicating that the complexation process is more favorable in methanol than in water. The Gibbs free energy of solvation for methanol and water were calculated, corresponding to −48.82 kcal/mol and −49.60 kcal/mol, respectively. These values suggest that the complex has more affinity to the solvent water, which implies stronger attractive forces between the solute and solvent in water than in methanol [48].

Alongside the binding and angle parameters, the geometry optimization reveals that $[Cu(Gln)(phen)(H_2O)]^+$ complex adopts a distorted square pyramidal geometry. This optimized structure shows a strong agreement with the experimental data. Therefore, given the great estimate achieved for almost all geometric parameters in an isolated monomer under different conditions, it will be possible to perform a good electronic properties' study and a reliable vibrational analysis of intramolecular vibration modes.

Therefore, the study of electronic properties was conducted from the optimized geometries obtained to determine chemical reactivity indices. The parameters were estimated from the frontier molecular orbitals (HOMO- LUMO) [49]. Using some mathematical relationships and energies of HOMO-LUMO, the following quantum-chemical descriptors are determined: energy gap (ΔEg), ionization potential (IP), electron affinity (EA), electronegativity (χ), chemical potential (μ), chemical hardness (η), softness (ς), and electrophilicity index (ϖ). The calculated values of reactivity indices for the $[Cu(phen)(Gln)(H_2O)]^+$ complex are shown in Table 1.

Since the complex is an open shell system, the gap HOMO-LUMO (ΔEg) is calculated considering alpha (α) and beta (β) orbitals. Thus, the true HOMO in solvents is α-HOMO, and the LUMO is β-LUMO; whereas in vacuum, the true HOMO and LUMO are α-HOMO and α-LUMO, respectively [2]. According to the data presented in Table 1, the highest values for α-HOMO and β-LUMO are observed in water and methanol, suggesting a significant solvation effect on the energies of the orbitals.

Besides that, high energy values related to the HOMO descriptor indicate greater electron-donating capacity, while low energies of LUMO describe lower resistance in accepting electrons [50,51]. The ΔEg is related to the electronic stability of a molecular system, since occurrence of an electronic transition is more difficult when the ΔEg is high [51]. The values of ΔEg calculated for the $[Cu(Gln)(phen)(H_2O)]^+$ complex in water and methanol are 4.72 eV and 4.71 eV, respectively. Also, the energies of HOMO and LUMO are related to the ionization energy and electron affinity descriptors. Specifically, the ionization energy is the energy needed to remove an electron from a complex; while the electron affinity corresponds to the energy change of a complex when an electron is added to it [52].

The electronegativity index indicates the ability of the complex to attract electrons [53]. Here, the electronegativity index is obtained, and three positive values are determined for the different conditions considered. The electronegativity decreases in the following order: vacuum > methanol > water. This trend indicates an increase in the wavelength of excitation energy in the same sequence [1].

Hardness describes the resistance to a distortion of the electron cloud of the system under an external influence [54]; while softness is the inverse of hardness, and both of these parameters were calculated herein. From an analysis of Table 1, we observe that the calculated values suggest that the $[Cu(Gln)(phen)(H_2O)]^+$ complex is most stabilized in methanol and water due to its relatively high hardness, indicating that the system has significant resistance to an electron cloud distortion, which also makes an influence on the ease for losing electrons [55].

Another quantum descriptor derived from frontier molecular orbital energies is the electrophilicity index. This parameter indicates the tendency of a chemical system to accept electrons [56]. It is also associated with a decrease in energy due to the optimal flow of electrons between the donor and acceptor sites. For the $[Cu(Gln)(phen)(H_2O)]^+$ complex in methanol, the electrophilicity index is 5.52 eV, suggesting that it can act as an electrophile, which implies that the complex may exhibit significant biological activity. The electrophilicity values found in this study are higher than those reported for other copper complexes with different ligands [57,58], including the well-known cisplatin complex [59,60], an antitumoral drug commonly used in cancer treatment [60–62].

In addition to the chemical reactivity indices presented above, an important property calculated is the dipole moment, which is associated with electronic mobility in a molecular system from the distribution of positive and negative partial charges [63]. Thereby,

Table 1
Chemical reactivity indices of $[Cu(Gln)(phen)(H_2O)]^+$ complex using PB1PBE functional and 6–31++G(d, p) and SDD computational levels.

Descriptor	Equation	Medium (eV or *1/eV*)		
		Vacuum	Methanol	Water
HOMO	–	−9.53	−7.46	−7.41
LUMO	–	−5.54	−2.74	−2.69
ΔEg	LUMO – HOMO	3.99	4.71	4.72
IP	– HOMO	9.53	7.46	7.41
EA	– LUMO	5.54	2.74	2.69
χ	– ½ (LUMO + HOMO)	7.54	5.10	5.05
μ	½ (LUMO + HOMO)	−7.54	−5.10	−5.05
η	½ (LUMO – HOMO)	1.99	2.36	2.36
ς	$1/2\eta$	0.25*	0.21*	0.21*
ϖ	$\mu^2/2\eta$	14.25	5.52	5.40

the dipole moment of $[Cu(Gln)(phen)(H_2O)]^+$ complex was calculated in vacuum, methanol, and water, whose values found are 7.17, 23.21, and 21.87 D (Debye), respectively. Our findings for the dipole moment values in methanol and water solvents indicate that the complex allows a high electron flux and potential biological activity. As noticed, the dipole moment is most pronounced in methanol.

According to our previous research [1,50], the calculated dipole moment of $[Cu(L\text{-methionine})(phen)H_2O]^+$ complex in water solvent is 18.51 D [50], whereas for the $[CuCl(glycine)(phen)]^+$ complex is 20.17 D [1], which differ of the dipole moment calculated herein for the $[Cu(Gln)(phen)(H_2O)]^+$ complex, also in water, whose value found is 21.87 D. It was noticed that the dipole moment estimated for the $[Cu(L\text{-methionine})(phen)H_2O]^+$ complex in vacuum is 13.52 D [50], while the value obtained in our study is found to be 7.17 D. Thus, it is noteworthy that the amino acid type affects the dipole moment of metal-organic complexes since this modification can be caused by polarity of the amino acids, as methionine and glycine are considered nonpolar, and glutamine is a polar substance. Table 2 gives the dipole moment values from the literature and those we obtained in this work.

To investigate the reactive sites of the $[Cu(Gln)(phen)(H_2O)]^+$ complex, electrostatic potential maps (EPMs) were predicted under different solvation conditions. Fig. 2a-c shows the contour surface divided into a pattern of warm colors (red, orange, and yellow) that characterize negative regions and cool colors (blue and green) characterizing positive regions. It is noticed that little changes are observed between EPMs calculated in water and methanol when compared to EPM calculated in vacuum. The negative are primarily concentrated over the nitrogen and oxygen atoms in the phen and Gln ligands, respectively, suggesting that these sites are nucleophilic. Besides that, the remaining EPM regions of the monomer exhibit charge depletion, which indicates their electrophilic character. From this electronic study, it is noticeable that these sites of the $[Cu(Gln)(phen)(H_2O)]^+$ complex also tend to participate in intermolecular interactions that can occur between the complex and other systems, including biomolecules.

3.3. Hirshfeld surfaces, 2D-fingerprint plot, and crystal voids studies

To complement the geometric and electronic properties of the $[Cu(Gln)(phen)(H_2O)]^+$ complex via DFT calculations, as we presented above, the intermolecular interactions occurring in the $[Cu(Gln)(phen)(H_2O)]NO_3{\cdot}H_2O$ crystal (Fig. 3a) were analyzed in detail using Hirshfeld surfaces and their analogs. Fig. 3b exhibits the three-dimensional pattern obtained from a ternary color gradient, in which the red, white, and blue regions correspond to intense, intermediate, and weak (null interactions), respectively [64]. As observed, the main contacts involve the oxygen atoms present in H_2O and Gln molecules, as well as nitrogen atoms belonging to the amino acid. The whitish sites mainly centered on the phen portion are associated with less intense contacts established between aromatic rings and neighboring units.

Fig. 3c-d exhibits the Hirshfeld surface in relation to the d_e and d_i, which represent distances in the boundary area on the outer and inner atoms of crystalline complex lattice, respectively. In d_e, regions in warm tones represent the sites related to the intermolecular interactions, while in d_i, this same color pattern indicates sites responsible for making contact between monomers. Complementarily, the surfaces shown in Fig. 3e–f characterize topological contacts, which are used to identify molecular packing between adjacent molecules, as well as their stacking in the crystal [65]. The shape index pictured in Fig. 3e illustrates the concave and convex sites of coordination complex represented by warm and cool colors, respectively. From this distribution, it is possible to notice where two $[Cu(Gln)(phen)(H_2O)]NO_3{\cdot}H_2O$ complex units touch each other via intermolecular interactions through which structural stability can be evaluated. Furthermore, the flat green areas and blue contours indicate low and high areas of curvatures, respectively, as shown in Fig. 3f, duly picturing the behavior of hardness surface. The intermolecular contacts constructed between complex units through the areas divide the surface.

In addition to the qualitative analysis of sites where intermolecular interactions occur, the 2D-fingerprint graphs are provided herein, as displayed in Fig. 4. This quantitative study allowed us to determine different types of contacts that stabilize the crystalline lattice based on the attraction and repulsion between molecular fragments constituents of the complex. Fig. 4a presents the cumulative 2D-fingerprint plot for the $[Cu(Gln)(phen)(H_2O)]NO_3{\cdot}H_2O$ crystal, in which the percentages are indicated and shown as a function of d_e and d_i properties characterized by a portion of points over the surface. The presence of blue dots indicates that the crystal is stabilized by high percentages of distant contacts between complex units. The full graph was decomposed from this pattern into stratified histograms corresponding to the specific intermolecular interactions with their percentages, as shown in Fig. 4b-i.

The H···O/O···H (36.6 %), H···H (36.1 %), and H···C/C···H (11.6 %) contacts contribute to more than 84.0 % of the Hirshfeld surfaces, showing that these intermolecular interactions confer the ordering of $[Cu(Gln)(phen)(H_2O)]NO_3{\cdot}H_2O$ complex units on the crystal lattice, as shown in Fig. 4b-i. Additionally, the sharp and high peaks observed in regions of low d_e and d_i values in the histograms indicate that the H···O/O···H and H···H present strong interactions in the crystal structure, as illustrated in Fig. 4b. Beyond that, less intense dispersive forces were also quantified as types: induced dipole (C···C, 5.3 %; O···O, 3.4 %), dipole-dipole (O···C/C···O, 1.6 %; N···O/O···N, 1.5 %), and hydrogen bonds (H···N/N···H, 2.9 %).

Table 2
Comparison between dipole moment values of $[Cu(Gln)(phen)(H_2O)]^+$ complex of this work and dipole moment values for other coordination complexes previously reported in the literature.

Complex	Amino acid	Theoretical dipole moment (Debye)	
		Water	Vacuum
$[Cu(L\text{-methionine})(phen)H_2O]^+$	Methionine	18.51 [45]	13.52 [45]
$[CuCl(glycine)(phen)]^+$	Glycine	20.17 [1]	–
$[Cu(Glutamine)(phen)(H_2O)]^+$	Glutamine	21.87	7.17

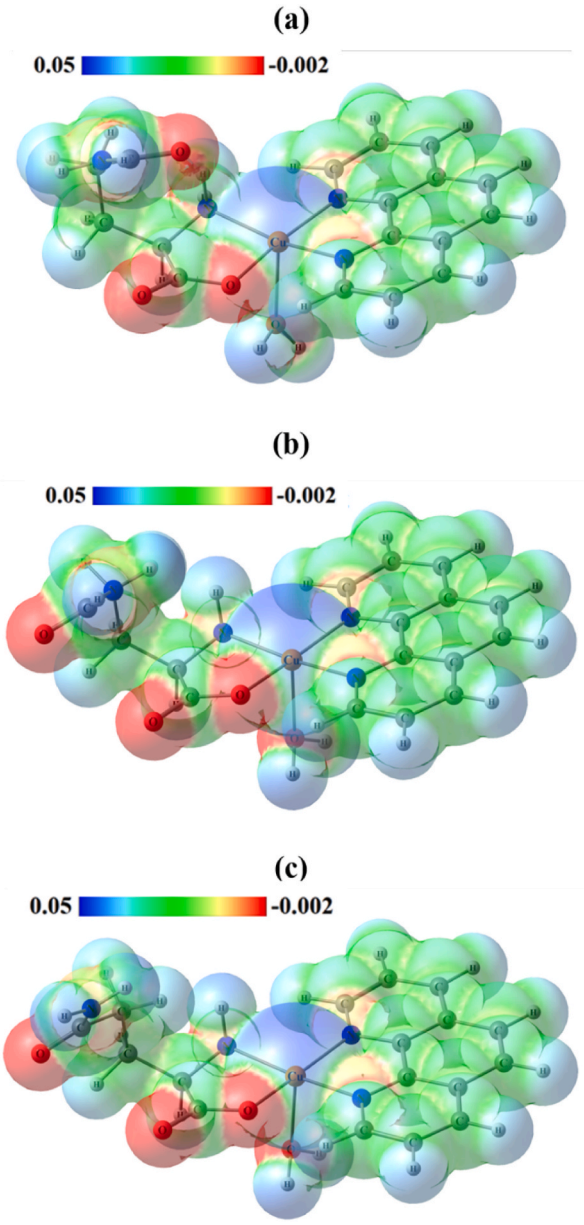

Fig. 2. Electrostatic potential maps (EPMs) of $[Cu(Gln)(phen)(H_2O)]^+$ complex in different conditions: (a) vacuum, (b) water, and (c) methanol.

A more detailed model of how intermolecular contacts are involved between $[Cu(Gln)(phen)(H_2O)]NO_3{\cdot}H_2O$ complex fragments is shown in Fig. 5. The red and green dashed lines represent H···O/O···H and H···H interactions, respectively. This behavior strengthens the results discussed above (Fig. 4b-c), highlighting that the main bonds involved between coordination complex units are hydrogen bondings, which contribute substantially to the stability of the complex analyzed herein [20].

Complementarily, another computational analysis was carried out in the $[Cu(Gln)(phen)(H_2O)]NO_3{\cdot}H_2O$ crystal (Fig. S3a of supplementary material) to investigate the crystal voids. Vacancies in the structural lattice are illustrated using electron density isosurfaces, as shown in Fig. S3b of supplementary material. These calculations provided an estimate of the free volume of primitive unit cell to be approximately 74.13 $Å^3$, which is equivalent to a percentage near 7.6 %. This value is considered low, and it is related to good stability in lattice energy, since systems exhibiting higher percentages (>15 %) of voids have a reduction in the energy of interactions and, consequently, their physicochemical properties can be affected, such as solubility, dissolution, and hardness [66]. Furthermore, the sites are not surrounded by isosurfaces, showing an area nearly 289.16 $Å^2$. These regions characterize areas where intermolecular contacts occur.

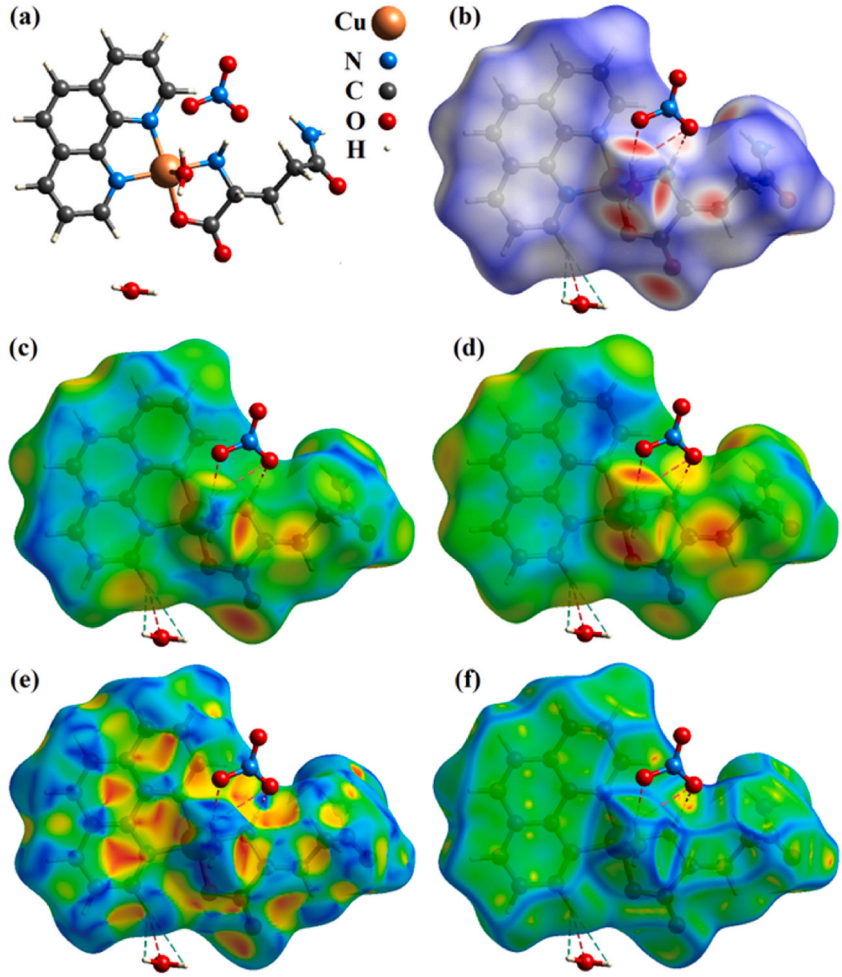

Fig. 3. (a) Molecular unit of [Cu(Gln)(phen)(H_2O)]NO_3·H_2O coordination complex. Hirshfeld surface of [Cu(Gln)(phen)(H_2O)]NO_3·H_2O complex mapped according to the (b) d_{norm}, (c) d_e, and (d) d_i, (e) shape index, and (f) curvedness.

3.4. Thermal analysis studies

Thermal behavior of powdered [Cu(Gln)(phen)(H_2O)]NO_3·H_2O crystals was investigated by TG and DTA analyses, as seen in Fig. 6. Thermal-TG curve shows thermal decomposition of the material occurs at three stages: (I) between 314 and 403 K, a mass loss around 6.6 % (34.77 g mol^{-1}) occurs due to release of two H_2O molecules, one free and other of coordination. In addition, the three endothermic peaks appearing at about 341, 369 and 398 K in the DTA curve are related to a dehydration process corresponding to the changes from the hydrate phase to anhydrous phase of [Cu(Gln)(phen)(H_2O)]NO_3·H_2O crystal; (II) between 403 and 623 K, a large mass loss corresponding to 42.4 % (206.51 g mol^{-1}) appears due to the decomposition from the free NO_3^- molecule and the fragmentation of organic species of the complex, since it needs more than one stage for total decomposition. An exothermic peak that appears near 506 K confirms this partial decomposition process, intermediate compounds formed, such as ammonia, carbon dioxide, carbon monoxide, among others, when evaporated release energy and they can propitiate exothermic events [67]; (III) above 623 K, a sharp decline is observed in the TG curve, another mass loss corresponding to 23.4 % (114.13 g mol^{-1}), which characterizes the decomposition of remaining carbon chains [68]. Concomitant to this last stage, a variation in the baseline of the DTA curve occurs suggesting a change in the specific heat of the sample due to the increase in temperature. This event is connected to appearance of an exothermic peak in the DTA curve ~673 K owing to carbonation of organic compound [68], followed by partial oxidation of the metal ion [1]. Table 3 provides the thermodynamic parameters obtained from the thermal analyses of powdered [Cu(Gln)(phen)(H_2O)]NO_3·H_2O crystals.

Fig. S4 (supplementary material) shows the DSC curve, which corroborates the TG and DTA results. The first three events observed at temperatures approximately 331, 361 and 384 K are caused by evaporation of water present in the crystalline complex. The enthalpies of the thermal events were determined, respectively, to be near 18.81 kJ/mol, 39.95 kJ/mol, and 7.28 kJ/mol. Therefore, the total enthalpy associated with the dehydration process is approximately 66.04 kJ/mol. In previous studies, dehydration enthalpy of monohydrated asparagine was reported to be ~49.7 kJ/mol [69] and the hemihydrated 5-methyluridine was obtained ~48.8 kJ/mol

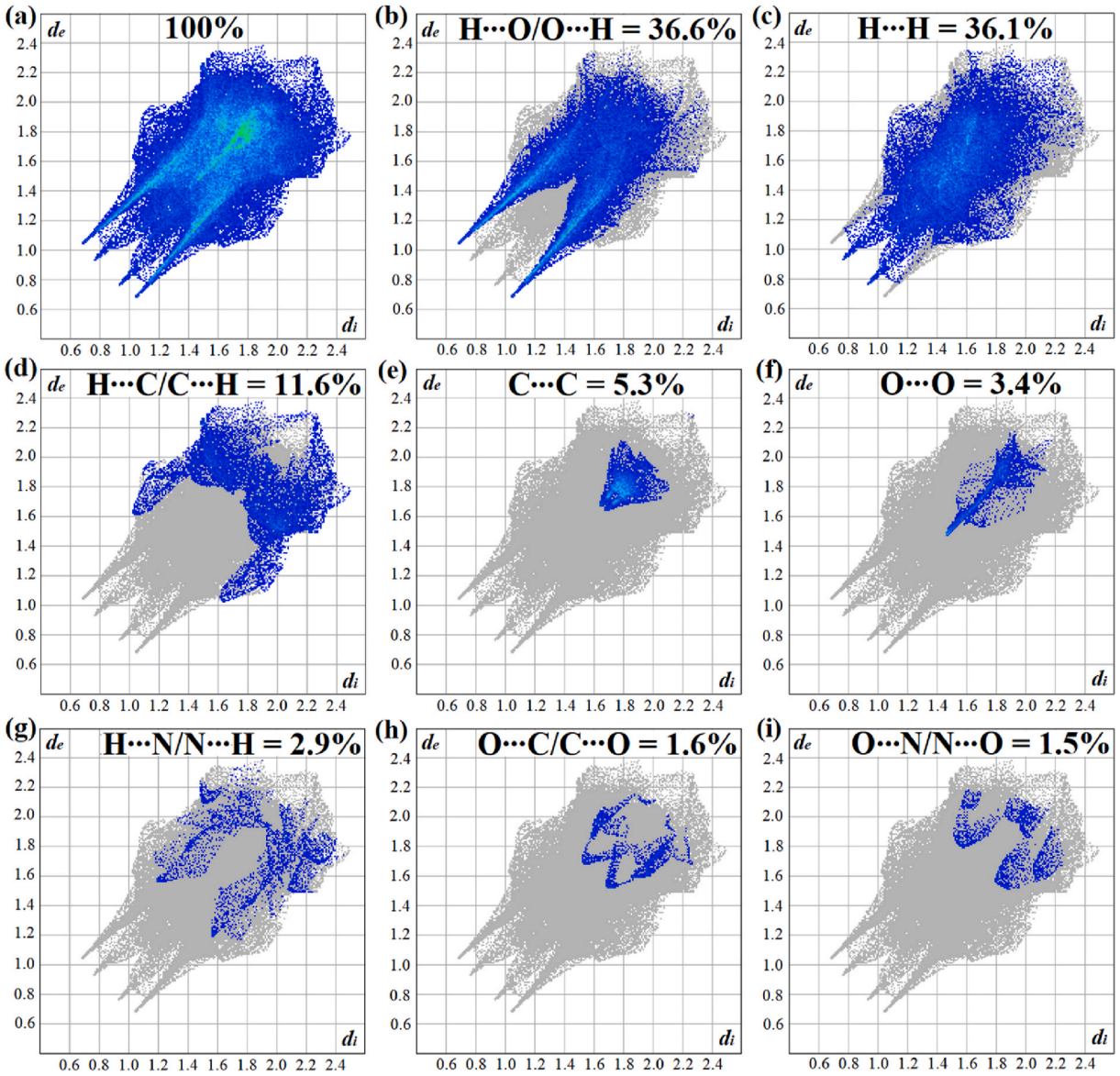

Fig. 4. (a) Cumulative 2D-fingerprint plot of [Cu(Gln)(phen)(H_2O)]NO_3·H_2O complex. Interaction-specific fingerprint plots: (b) H···O/O···H, (c) H···H, (d) H···C/C···H, (e) C···C, (f) O···O, (g) H···N/N···H, (h) O···C/C···O, and (i) O···N/N···O.

[70]. These values are corresponding to the vaporization of water, which is around 41 kJ/mol [67–71]. Energy difference of 24.64 kJ/mol between water vaporization and [Cu(Gln)(phen)(H_2O)]NO_3·H_2O crystals dehydration can be attributed to the intermolecular interactions of water in the crystal lattice, indicating that the significant role of H_2O molecules is essential to the crystal structure. Furthermore, the thermal event noticed near 498.9 K with enthalpy of 97.29 kJ/mol occurs due to the partial decomposition of organic compounds, also indicating the formation of intermediate compounds, which are in agreement with the TG/DTA results.

3.5. FT-IR and Raman spectroscopy studies

As previously related by Kiraz et al. [28] and according to the PXRD study performed herein, the unit cell of [Cu(Gln)(phen)(H_2O)]NO_3·H_2O complex contains 52 atoms and 2 formulas, totaling 104 atoms and, therefore 312 degrees of freedom. Furthermore, it was verified that the crystal phase corresponds to triclinic structure with C_i^1 group. According to theory [72], the representation describing the Raman and IR modes are associated with C_i-factor group is $\Gamma = 3A_g + 3A_u$, where the fundamental vibrations for both Raman and IR activities correspond to A_g and A_u, respectively. As each pair of atoms occupies C_i-site symmetry within the primitive cell, the occupied sites are a total of 52 resulting in a total of vibration normal modes given by $\Gamma^{total} = 156A_g + 156A_u$. However, among them,

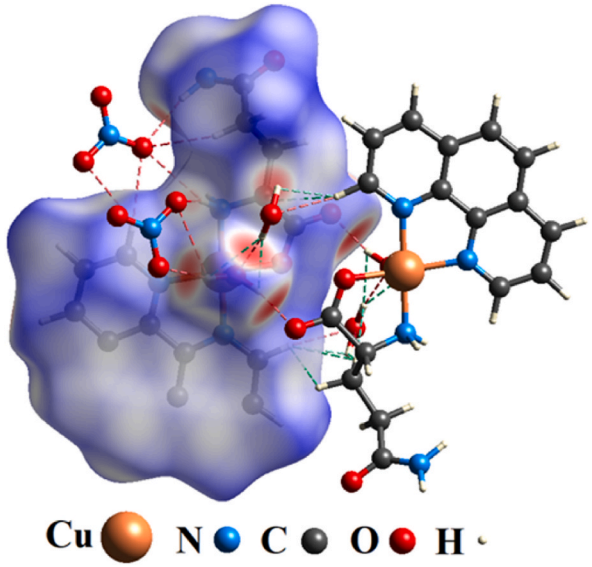

Fig. 5. Intermolecular contacts in the $[Cu(Gln)(phen)(H_2O)]NO_3{\cdot}H_2O$ complex: red (H···O/O···H), and green (H···H) dashed lines.

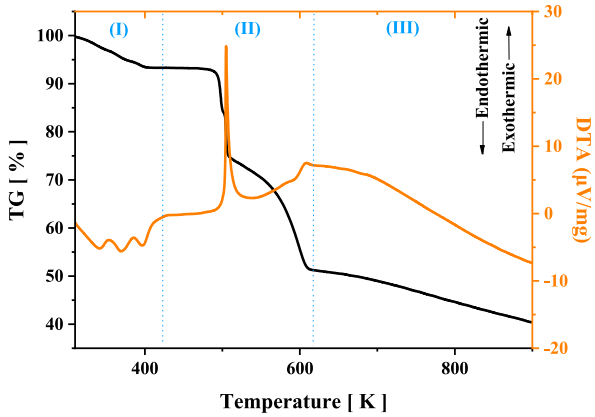

Fig. 6. TG and DTA curves of powdered $[Cu(Gln)(phen)(H_2O)]NO_3{\cdot}H_2O$ crystals obtained in the temperature interval of 300–900 K.

Table 3
Thermal events and thermodynamic parameters of powdered $[Cu(Gln)(phen)(H_2O)]NO_3{\cdot}H_2O$ crystals.

Regions	Temperature [K]			Weight [g.mol^{-1}]	Mass loss [%]	ΔH [kJ.mol^{-1}]
	T_{onset}	T_{peak}	T_{endset}			
I	330.2	355.2	279.6	34.77	6.6	−764.48
II	493.9	522.8	315.4	206.51	42.4	446.69
III	810.6	917.2	296.4	114.13	23.4	−4572.27

the acoustic modes are given by $\Gamma^{ac} = 3A_u$; therefore $\Gamma^{Raman} = 156A_g$ are Raman, and $\Gamma^{IR} = 153A_u$ are IR modes.

Theoretical vibrational properties of $[Cu(Gln)(phen)(H_2O)]^+$ complex are combined with experimental Raman and IR studies from the better geometry optimized by DFT, which was obtained using PBE1PBE functional. The intramolecular modes are calculated and assigned from distinct conditions. Figs. 7 and 8 show the experimental (IR and Raman) spectra, respectively, at room temperature in the wavenumber regions of 4000–400 cm^{-1} and 40–3200 cm^{-1}, respectively. As noticed in both figures, the confrontation between the experimental spectra and predicted spectra obtained in methanol, water, and vacuum is provided for a better analysis. Experimental results from vibrational spectroscopy agree well with theoretical data. In addition, all IR and Raman bands' positions in cm^{-1} with their respective assignments are given in Tables S2 and S3 (supplementary material).

Six vibration modes are recorded in the Raman spectrum at about 58, 77, 110, 135, 170, and 180 cm^{-1} (*insert* of Fig. 8a), they

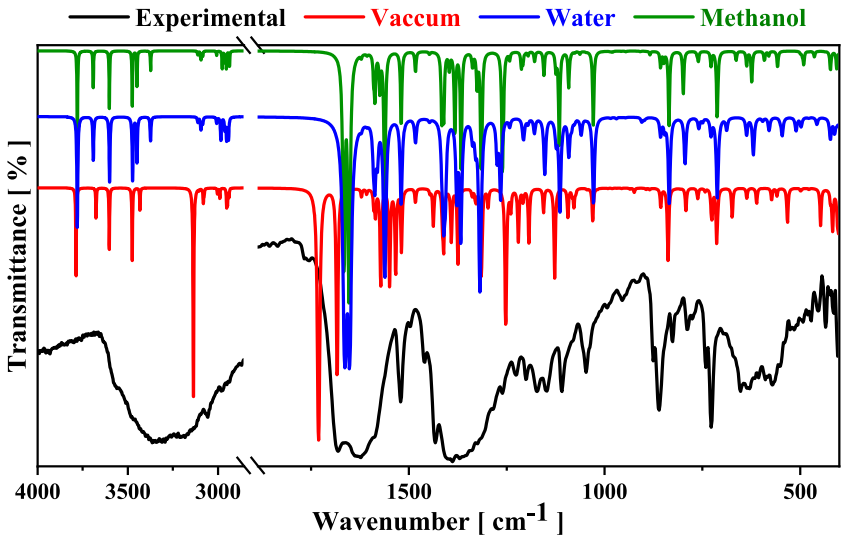

Fig. 7. Comparison between experimental (black) and calculated IR spectra in water methanol (green) and (blue) solvents, and vacuum (red) conditions, using DFT/PBE1PBE computational level for the $[Cu(Gln)(phen)(H_2O)]^+$ complex.

belong to the crystalline lattice vibrations. Generally, lattice vibrations are coupled with hydrogen bonds' vibrations [50,73–75]. Additionally, vibrational motions owing to metal-ligand bonds appear below 590 cm^{-1} as low-intensity bands indicating the presence of bonds from copper with phen and Gln ligands. Thereby, in the spectral region of 510–200 cm^{-1} of the two spectra appear vibration modes due to bending, torsion, and stretchings from the metal and ligands. On the other hand, the low-intensity band noticed nearly 250 cm^{-1} in the Raman spectrum is attributed to the bending from the aromatic ring of phen ligand. Interestingly, the peak position of this band is well stable for the different conditions used in the PCM-DFT vibrational calculations. According to our calculations, two Raman bands near 292 and 316 cm^{-1} are described as bending motions involving Cu–N–C and N–Cu–O bonds, respectively. In three different conditions, an experimental Raman band around 508 cm^{-1} is associated with combined vibrations of Cu–N stretching and CCO stretching from the phen and Gln molecular portions. Regarding this band, a little change is observed between experimental and theoretical peak positions (498, 499, and 501 cm^{-1}) in different mediums utilized in our PCM-DFT predictions.

The experimental IR band observed at about 411 cm^{-1} corresponding to the bending of Cu–O–H. The low-intensity IR bands centered at 469 and 550 cm^{-1} are assigned as combined motions of torsion and bending vibrations of the Cu–N–C–C dihedrals, and in the coordination sphere involving the Cu–N–C bond, with very low contribution of carbon chain from the phen and Gln portions. The corresponding theoretical IR peaks' positions at vacuum and water mediums present notable redshift in relation to the two experimental peaks (469 and 550 cm^{-1}). Additionally, experimental bands centered at 562 (Raman) and 586 (IR) cm^{-1} are due to combined motions of C–C stretching and deformation of COO unit, respectively. The Raman band observed nearly 739 cm^{-1} is assigned as a combination of stretching's of C–C and C–N of the molecular structure of Gln. The PCM–DFT theoretical peak position calculated at methanol shows a large blue shift in relation to the experimental position. IR band observed near 650 cm^{-1} is due to C–C–C deformation and C–C stretching of amino acid. It is worth highlighting that when the peaks' positions calculated at three different conditions are compared to those experimental peaks' positions due to the motions from the structure of Gln, one can notice that the dielectric mediums strongly affect its PCM-DFT calculated modes, corroborating the structural modifications on the coordination complex, as observed in Fig. S3 of supplementary material. All IR and Raman peaks' positions and assignment of intramolecular modes are provided in Tables S2 and S3 (supplementary material).

Vibration bands within 740–1400 cm^{-1} region are associated with combined motions by several stretching and deformations of chemical units of the phen and Gln ligands. The Raman modes noticed nearly 723, 854, 1045, 1021 and 1523 cm^{-1} are due to bending of aromatic rings of the phen ligand. Besides that, IR absorption modes observed around 723, 773, 824, 858, 989, 1120, and 1198 cm^{-1} are also associated with bending of aromatic rings of the phen structure. Our calculations also allowed us to infer that IR bands between 870 and 1400 cm^{-1} are due to combined motions mainly related to the stretching and bending involving the CC, CCH, CN, CO_2, CH_2, and NH_2 units from the Gln ligand. Among all these vibrations, it is important to highlight that the DFT-predicted modes at about 1376 and 1381 cm^{-1} due to γ(HCH)+ν(CC)+ν(CN) which were calculated, respectively, at water and methanol solvents, present a shift to low wavenumbers in relation to the experimental IR mode recorded near 1387 cm^{-1}. Considering the Raman observations in the 880–1400 cm^{-1} region, one can notice vibrations located at about 882, 1065, 1144, 1256, 1315, 1365, and 1389 cm^{-1} that correspond to a combination of motions of the stretching and deformation types of CH_2, NH_2, CO, CN, CC, HCC, and HCN units from the Gln structure. In the PCM-calculated bands under water and methanol solvents when compared to two experimental bands recorded at about 1144 and 1256 cm^{-1}, corresponding to the ν(C=O)+δ(HCH)+δ(HNH) and ν(C–O)+ν(C–N) vibrations, one can note a shift to high wavenumbers. This fact is due to the direct participation of hydrogen bonds in these vibration modes [17,76–78]. In IR and Raman spectra between 1400 and 1590 cm^{-1} were recorded a set bands due to CC- and CN-stretching vibrations along with a contribution of ring bending, $\delta(phen_{ring})$, from the Gln and phen ligands.

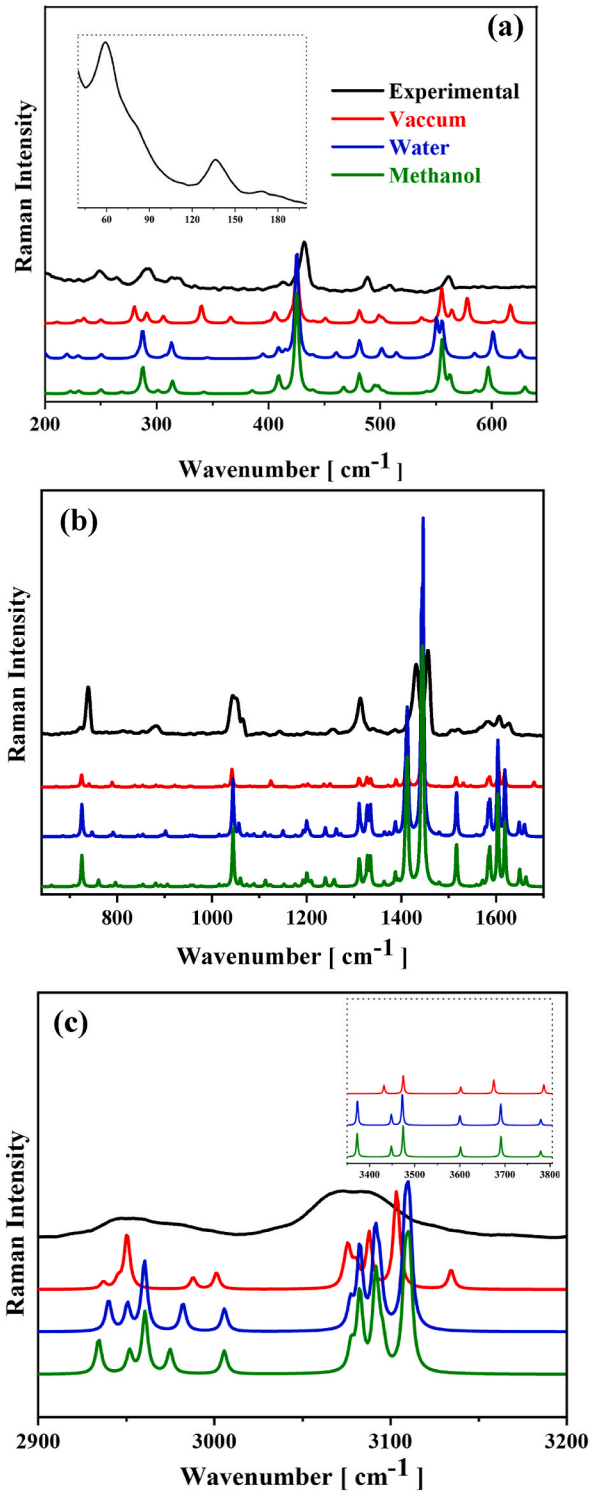

Fig. 8. Comparison between experimental (black) Raman spectrum and the calculated IR spectra in methanol (green), water (blue), and vacuum (red) conditions using DFT/PBE1PBE computational level for the $[Cu(Gln)(phen)(H_2O)]^+$ complex in the regions: (a) 40–650 cm^{-1}, (b) 650–1650 cm^{-1}, and (c) 2900–3200 cm^{-1}. The *inset* is theoretical spectral region of 3350–3800 cm^{-1} in methanol (green), water (blue), and (red) vacuum.

Particularly, an important vibrational analysis is related to the motion of C=O unit under solvation medium. Table S2 provides two Raman modes located nearly 1622 and 1680 cm^{-1} are due to ν(C=O) stretching and combined stretchings of C=O and C–O units of the polar portion of Gln. PCM-calculated mode at water and methanol solvents present strong shifts to low wavenumbers with $\Delta\omega = 29$ and 28 cm^{-1}, when compared to the experimental mode at higher wavenumber (1680 cm^{-1}).

In addition, the doublet corresponding to the IR modes around 1636 and 1680 cm^{-1} are due to a combination of stretching motions of C–O, C-N and C=O units. In relation to the first experimental mode (1636 cm^{-1}), the DFT-predicted modes at water (1651 cm^{-1}) and methanol (1652 cm^{-1}) suffer displacements to high wavenumbers whose variations are $\Delta\omega = 15$ and 16 cm^{-1}, respectively. Nevertheless, we compared the calculated modes at water (1663 cm^{-1}) and methanol (1665 cm^{-1}) with second experimental mode (1680 cm^{-1}), at which are noticed shifts to low wavenumbers which are found to be $\Delta\omega = 17$ and 15 cm^{-1}, respectively. From this analysis, one can note that the solvents affect the intramolecular bands that have direct connection with intermolecular forces due to the presence of hydrogen bonds [17,76], showing that the molecular portion most affected is the fragment of Gln.

The interactions owing to carbonyl of Gln and oxygen of the water is a strong hydrogen bond [17,77]. Under aqueous medium, water can connect to the oxygen atoms of glutamine through hydrogen bonds, leading to a red shift in the vibrational wavenumber of the carbonyl unit. The hydrogen atoms of Gln act as bond receivers, favoring the intermolecular forces due to hydrogen bonds in the lattice formed by water. This phenomenon is related to the changes noticed in the N–H stretching's around 3508 cm^{-1} and the deformation of NH_2 near 1570 cm^{-1}, which can couple to other motions related to the vibration modes of amino acid. Theoretical IR and Raman bands show changes caused by the solvents, indicating the formation of new intermolecular interactions.

At high-wavenumber region within 2800–3600 cm^{-1}, vibration bands that appear in both IR and Raman are mainly associated with stretching's of the CH, CH_2, CH_3, and NH_2 units due to phen and Gln ligands. Specifically in this spectral region, the calculated modes at different solvation conditions present the smallest wavenumber deviations when compared with the experimental vibration modes analyzed herein. In Raman spectrum, the low-intensity bands around 3769 and 3688 cm^{-1} are related to the anti-symmetric and symmetric stretching's of H_2O that contributes to the coordination compound.

3.6. UV–Vis–NIR spectroscopy studies

Fig. 9 shows the experimental UV–Vis absorption spectra in the region of 200–1100 nm for the $[Cu(Gln)(phen)(H_2O)]NO_3{\cdot}H_2O$ complex in methanol and water solvents. The behavior of electronic absorption indicates that the bands noticed between 200 and 400 nm are associated with the internal electronic transitions of the π–π^* type referring to the ligands [55]; while the very broadband recorded from 400 to 1100 nm for the complex in both solvents is characteristic of *d*–*d* transitions. Further, the behavior associated with this band is connected to the overlapping of three smaller bands corresponding to the $^2B_{1g} \rightarrow {}^2A_{1g}$, $^2B_{1g} \rightarrow {}^2B_{2g}$, and $^2B_{1g} \rightarrow {}^2E_g$ transitions, which are characteristic of pentacoordinate copper complexes [79], and allowed by spin and prohibited by Laporte [80]. A comparison between two absorption spectra measured in both solvents allows to note that the bands show slight shifts. This behavior is attributed to solvent polarity, which is a physicochemical property that affects the absorption wavelength of metal complexes.

3.7. Cytotoxic activity

To evaluate the anticancer potential of $[Cu(Gln)(phen)(H_2O)]NO_3{\cdot}H_2O$ complex, cytotoxicity assays were conducted on two cell lines: prostate (PC-3) and glioblastoma (SNB-19). The results obtained through IC_{50} and SI parameters are given in Table 4. Notably, the complex demonstrates inhibitory effects on both cell types, with IC_{50} values of 3.3 (2.6–4.1) μM for PC-3 cells and 3.8 (3.3–4.6) μM for SNB-19 cells. This cytotoxic activity is more potent than other studies, including docetaxel [81] and phen:copper complex combined with asparagine or methionine [2]. In addition, the standard drug, cisplatin, had IC_{50} values of 4.8 (3.3–7.0) μM for PC-3 cells

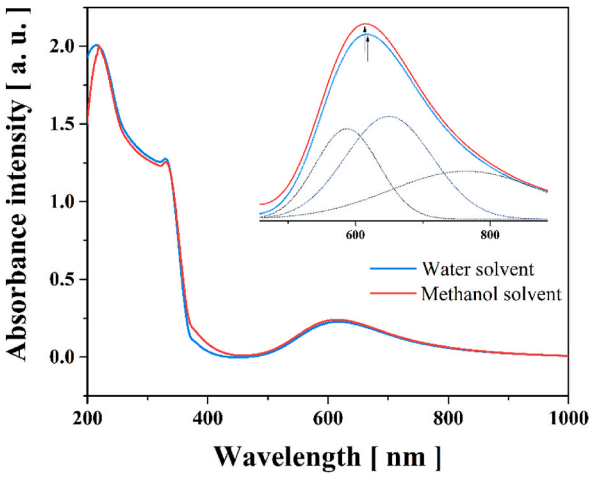

Fig. 9. UV–Vis–NIR absorption spectra of $[Cu(Gln)(phen)(H_2O)]NO_3{\cdot}H_2O$ complex in aqueous and methanolic mediums.

Table 4
IC_{50} (μM) and SI values obtained for the PC-3, SNB-19, and RAW-264.7 cell lines treated with $[Cu(Gln)(phen)(H_2O)]NO_3{\cdot}H_2O$ complex for 72 h.

Cell line	Histotype	[a]IC_{50} μM (CI 95 %)/SI	
		$[Cu(Gln)(phen)(H_2O)]NO_3{\cdot}H_2O$	Cisplatin
PC3	Prostate	3.3 (2.6–4.1)/1.3	4.8 (3.3–7.0)
SNB19	Glioblastoma	3.8 (3.3–4.6)/1.1	2.9 (2.3–3.6)
RAW 264.7	Macrophage	4.2 (3.8–4.6)	–

CI 95 %: Data are presented as IC_{50} values and 95 % confidence interval.
S.I.: Selectivity index - IC_{50} value in the non-tumor cell line (RAW 264.7) divided by the IC_{50} value in the tumor cell lines.
[a] IC_{50}: Half-maximal inhibitory concentration.

and 2.9 (2.3–3.6) μM for SNB-19 cells. These data indicate that $[Cu(Gln)(phen)(H_2O)]NO_3{\cdot}H_2O$ complex has superior efficacy in relation to the cisplatin for PC-3 cells.

The cytotoxicity of $[Cu(Gln)(phen)(H_2O)]NO_3{\cdot}H_2O$ crystals was further evaluated on the non-cancerous cell line (RAW-264.7). The IC_{50} value observed was 4.2 (3.8–4.6) μM. Comparing this result with IC_{50} values for the cancer cells, the selectivity indices were 1.3 for PC-3 and 0.9 for SNB-19. These data suggest that the complex demonstrates significant selectivity towards both cancer cell lines, with a slightly higher preference for the PC-3 cells.

The selectivity for the unhealthy cells can be attributed to mutation observed in cancer cells. These alterations promote interactions between plasmatic membrane (or DNA) and complex. Normally, the uptake of Cu^{2+} into cells is regulated by specific proteins in the plasma membrane [82]. However, the coplanarity of the phen molecule enhances its leading to increased ion permeability within the cells [83]. These data suggest that the complex demonstrates significant selectivity towards both cancer cell lines [84,85].

Additionally, it is well-understood that these metal-organic complexes can engage with a cell's DNA, releasing the Cu^{2+} ion [85,86]. The released ion is crucial for the formation of free radicals, which in turn cause damage to DNA, leading to cell apoptosis [85]. Importantly, this mechanism is more pronounced in tumorous cells. Due to their uncontrolled growth, the DNA of tumorous cells remains exposed for extended periods [87]. This prolonged exposure makes them more susceptible to the interactions with organic components of $[Cu(Gln)(phen)(H_2O)]NO_3{\cdot}H_2O$ crystals, thus explaining their heightened vulnerability. Finally, based on the study carried out on PC-3 and SNB-19 cell lines, we believe mutations in specific regulators such as TP53, PTEN and EGFR could contribute to the differences in cytotoxicity values.

3.8. ADME and drug-likeness

To provide more valuable information about the application of $[Cu(Gln)(phen)(H_2O)]^+$ complex in the area of anticancer drug development, a computational analysis via drug-likeness and ADME was performed. ADME method (*in silico*) was used to investigate whether the coordination compound synthesized here produces any toxicity after its possible administration in the human body or shows a pharmacokinetic profile [88]. Besides, the optimized geometries, as described in section 3.2 were used; however, all structures presented equivalent values. Nevertheless, due to the good affinity of this complex with water, we chose this solvation medium to discuss these results. The results obtained are given in Table S4 (supplementary material), with various parameters, including topological polar surface area (TPSA), lipophilicity, solubility, gastrointestinal (GI) absorption, blood-brain barrier (BBB) penetration, permeability glycoprotein (P-gp), pan assay interference compounds (PAINS), among others, were calculated.

Regarding the physicochemical properties, the complex exhibits a TPSA = 117.44 $Å^2$. This value aligns with established pharmacokinetic models indicating strong GI absorption, anyway, the compound is unable to cross the BBB [4]. Furthermore, the calculated lipophilicity is −4.43, which corresponds to the coefficient octanol/water partition coefficient (logP) of the complex. Additionally, the high lipophilicity demonstrates greater affinity of the compound with the aqueous phase, justifying the soluble class observed with a value near 1.78×10^{-2} mg/mL.

The P-gp factor indicates the ability of glycoproteins on the cell membranes to expel foreign substances from cells. According to our results, the complex exhibits the potential to function as a substrate in this process. In addition, it is known that enzymes related to cytochrome P450 enzymes facilitate the breakdown of drug molecules within cells, making them more polar and water-soluble [89]. The inhibitory data for five enzymes (CYP1A2, CYP2C19, CYP2C9, CYP2D6, and CYP3A4) associated with cytochrome indicate that the complex does not inhibit any CYP enzymes tested, indicating that oral administration of the complex poses no risk of hepatotoxicity. Furthermore, pharmacokinetics was ascertained in terms of skin permeability by Log*K*p. A lower *K*p value indicates reduced permeability of the complex through the skin [90], *i.e.*, the drug molecule cannot travel properly within the organism, does not undergo biotransformation, and may have low bioavailability. The obtained value is excessively negative ($Kp = -8.65$), suggesting that the complex cannot act as a permeator agent on the skin, *i.e.*, the complex cannot cross the barrier imposed by the skin.

Drug-likeness was evaluated based on Lipinski's rule of five [91]. These indicators provide a qualitative assessment of a molecule's potential to become an oral drug in terms of its bioavailability. Additionally, drug-likeness is determined by the structural and physicochemical properties of potential compounds. In this methodology, a routine is used to filter chemical libraries to exclude molecules with undesirable parameters with an acceptable pharmacokinetic profile. The analysis is performed on five different filters (Ghose – Amgen, Lipinski – Pfizer, Egan – Pharmacia, Veber – GSK and Muegge – Bayer), which aim to enhance the quality of the initial compound classes [39]. Interestingly, only Ghose's parameter is not violated, so to meet all criteria, $[Cu(Gln)(phen)(H_2O)]^+$ can act as a secondary drug associated with a drug already used to exhibit desired effects. The bioavailability score was 0.55. Values above 0.10

suggest that the compound can be used as a substrate via oral administration [91].

In addition, some alerts on medicinal chemistry properties for the $[Cu(Gln)(phen)(H_2O)]^+$ complex were also analyzed. The PAINS index provides information about the molecular fragment exhibiting a response against a protein target; however, this indicator was absent. The similarity with drugs that do not have aromatic rings in their structure was observed, such as molecules exhibiting the following chemical units: N–C–N, O–C–O, and S–C–S. Finally, synthetic accessibility is associated with the ease that the compound has in being reproduced in clinical pharmaceutical approaches. Values near 1 indicate a straightforward synthesis route, whereas values approaching 10 suggest more complex processes [89]. The value calculated for the $[Cu(Gln)(phen)(H_2O)]^+$ complex is 6.39, which is considered intermediate, suggesting a challenging synthesis with promising results.

4. Conclusions

In this study, the $[Cu(Gln)(phen)(H_2O)]NO_3{\cdot}H_2O$ crystals were characterized using both experimental and theoretical techniques. The geometric, electronic, chemical, and vibrational properties of the complex were evaluated and the biological activity was assessed. DFT calculations allowed a comprehensive understanding of these properties, confirming that the complex exhibits promising biological activity. Theoretical predictions under vacuum, aqueous, and alcoholic conditions showed that the physical and chemical characterizations of the complex were slightly influenced by the different dielectric environments, as observed through the IEFPCM method. Hirshfeld surface calculations allowed us to identify the regions involved in intermolecular interactions, determining percentage of contacts into the crystal lattice. Isosurfaces revealed the voids within unit cell. Thermal analyses indicated that the powdered $[Cu(Gln)(phen)(H_2O)]NO_3{\cdot}H_2O$ crystal undergo dehydration, which is linked to phase transformations owing to the loss of coordinated and free water. Theoretical intramolecular vibration modes were duly assigned, showing a good correlation with experimental data. UV–Vis–NIR analyses in aqueous and methanolic media demonstrated that the solvent affects the absorption wavelength of the complex. Furthermore, *in vitro* cytotoxicity assays suggested that the $[Cu(Gln)(phen)(H_2O)]NO_3{\cdot}H_2O$ crystal exhibits antitumor activity and selectivity against PC-3 and SNB-19 lines. *In silico* pharmacokinetic predictions indicated that the complex fits well within several models, displaying good gastrointestinal absorption, solubility, and no hepatotoxicity risk. Overall, our findings indicated that the $[Cu(Gln)(phen)(H_2O)]NO_3{\cdot}H_2O$ crystal is a cost-effective material with remarkably significant physical, chemical and cytotoxic features, making it an important candidate at therapies against cancer treatment.

CRediT authorship contribution statement

Marinaldo V. Souza Junior: Writing – review & editing, Writing – original draft, Visualization, Investigation, Funding acquisition, Formal analysis, Data curation. **João G. Oliveira Neto:** Writing – review & editing, Writing – original draft, Visualization, Validation, Software, Methodology, Investigation, Formal analysis, Conceptualization. **Walajhone O. Pereira:** Writing – original draft, Visualization, Software, Investigation, Data curation. **Jéssica A.O. Rodrigues:** Writing – review & editing, Validation, Methodology, Conceptualization. **Jailton R. Viana:** Writing – review & editing, Methodology, Formal analysis, Conceptualization. **Aramys S. Reis:** Writing – review & editing, Writing – original draft, Visualization, Validation, Supervision, Methodology, Formal analysis, Data curation, Conceptualization. **Mateus R. Lage:** Writing – review & editing, Writing – original draft, Visualization, Software, Methodology, Investigation, Formal analysis, Conceptualization. **Guilherme G.C. Carvalho:** Writing – review & editing, Visualization, Validation, Methodology, Investigation, Data curation. **Cláudia O. Pessoa:** Writing – review & editing, Writing – original draft, Visualization, Validation, Methodology, Investigation, Conceptualization. **Adenilson O. dos Santos:** Writing – review & editing, Writing – original draft, Resources, Methodology, Investigation, Conceptualization. **Francisco F. de Sousa:** Writing – review & editing, Writing – original draft, Visualization, Validation, Supervision, Resources, Project administration, Methodology, Investigation, Funding acquisition, Formal analysis, Conceptualization.

Declaration of competing interest

The authors declare the following financial interests/personal relationships which may be considered as potential competing interests:Francisco Ferreira de Sousa reports financial support and administrative support were provided by Federal University of Para. Francisco Ferreira de Sousa reports a relationship with Federal University of Para that includes: employment. If there are other authors, they declare that they have no known competing financial interests or personal relationships that could have appeared to influence the work reported in this paper.

Acknowledgments

The authors want to express their gratitude to the Brazilian agencies: Coordenação de Aperfeiçoamento de Pessoal de Nível Superior - Brazil (Finance Code – 001), Conselho Nacional de Desenvolvimento Científico e Tecnológico (CNPq, grant no. 312926/2020-0 and 308789/2022-9), and Fundação de Amparo à Pesquisa e ao Desenvolvimento Científico e Tecnológico do Maranhão (FAPEMA, Grants#: 00808/19, 44428/2022, and 12643/22) for their financial support. We extend our thanks to the partners who provided the resources necessary for computational calculations, particularly the national advanced computing platform Digital Research Alliance of Canada, through the account of Stanislav Stoyanov, Ph.D., Adjunct Professor of the Department of Chemical and Materials Engineering, University of Alberta, Edmonton, Alberta, Canada.

Appendix A. Supplementary data

Supplementary data to this article can be found online at https://doi.org/10.1016/j.heliyon.2024.e37505.

References

[1] J.G. de Oliveira Neto, J.G.S. Filho, E.M. Bittar, L.M. Silva, F.F. De Sousa, H.V. Domingos, L.V. Costa-Lotufo, A.S. Reis, A.O. Dos Santos, Structural, thermal, electronic, vibrational, magnetic, and cytotoxic properties of chloro(glycinato-N,O)(1,10-phenanthroline-N,N′)-copper(II) trihydrate coordination complex, J. Inorg. Biochem. 226 (2022) 111658, https://doi.org/10.1016/j.jinorgbio.2021.111658.

[2] J.A.O. Rodrigues, J.G. De Oliveira Neto, A.O.S. De Barros, A.P. Ayala, R.S. Oliveira, A.S. De Menezes, F.F. De Sousa, Copper(II): phenanthroline complexes with l-asparagine and l-methionine: synthesis, crystal structure and in-vitro cytotoxic effects on prostate, breast and melanoma cancer cells, Polyhedron 191 (2020) 114807, https://doi.org/10.1016/j.poly.2020.114807.

[3] D. Vušak, K. Ležaić, J. Jurec, D. Žilić, B. Prugovečki, Solvent effects on the crystallization and structure of ternary copper(II) coordination compounds with l-threonine and 1,10-phenanthroline, Heliyon 8 (2022) e09556, https://doi.org/10.1016/j.heliyon.2022.e09556.

[4] M.C. Ramos, J.G. de Oliveira Neto, C.E.S. Nogueira, A.S. Reis, F.F. De Sousa, L.M. da Silva, A.O. dos Santos, Structural, vibrational, thermal, and cytotoxic characterization of aqua(1,10-phenanthroline)(L-serinato)copper(II) nitrate complex combined with DFT calculations, Cryst. Res. Technol. n/ a (2023) 2300240, https://doi.org/10.1002/crat.202300240.

[5] J.A.O. Rodrigues, A.U. Torres, N.A.B. de Sousa, T.J.D. de Sousa, J.G.O. Neto, A.S. Reis, M.R. Lage, A.O. dos Santos, C.C. dos Santos, A.S. de Menezes, F.F. De Sousa, Synthesis, characterization, DFT study, and antibacterial activity of a coordination complex of Cu(II) with 1,10-phenanthroline and l-methionine ligands, J. Mol. Struct. 1293 (2023) 136197, https://doi.org/10.1016/j.molstruc.2023.136197.

[6] M.S.S. Adam, M.M. Makhlouf, F. Ullah, O.M. El-Hady, Mononucleating nicotinohydazone complexes with VO^{2+}, Cu^{2+}, and Ni^{2+} ions. Characteristic, catalytic, and biological assessments, J. Mol. Liq. 334 (2021) 116001, https://doi.org/10.1016/j.molliq.2021.116001.

[7] M.S.S. Adam, H. Elsawy, A. Sedky, M.M. Makhlouf, A. Taha, Catalytic potential of sustainable dinuclear (Cu^{2+} and ZrO^{2+}) metal organic incorporated frameworks with comprehensive biological studies, J. Taiwan Inst. Chem. Eng. 144 (2023) 104747, https://doi.org/10.1016/j.jtice.2023.104747.

[8] M. Azam, S.M. Wabaidur, M. Alam, Z. Khan, I.O. Alanazi, S.I. Al-Resayes, I.S. Moon, Rajendra, Synthesis, characterization, cytotoxicity, and molecular docking studies of ampyrone-based transition metal complexes, Transit. Met. Chem. 46 (2021) 65–71, https://doi.org/10.1007/s11243-020-00422-8.

[9] M. Shakir, N. Shahid, N. Sami, M. Azam, A.U. Khan, Synthesis, spectroscopic characterization and comparative DNA binding studies of Schiff base complexes derived from l-leucine and glyoxal, Spectrochim. Acta Part A Mol. Biomol. Spectrosc. 82 (2011) 31–36, https://doi.org/10.1016/j.saa.2011.06.035.

[10] M. Azam, S.I. Al-Resayes, M. Alam, A. Trzesowska-Kruszynska, R. Kruszynski, M.R.H. Siddiqui, A new ladder-type dichloro(2,2-dimethyl-1,3-diaminopropane) copper complex: synthesis, structural studies and selective sensing behavior towards a ketone molecule, Polyhedron 170 (2019) 287–293, https://doi.org/10.1016/j.poly.2019.05.053.

[11] G. Valora, G. Munzi, R.P. Bonomo, Ternary copper(II) complexes with 1,10-phenanthroline and various amino acids: a spectroscopic and voltammetric study in aqueous solution, J. Inorg. Biochem. 191 (2019) 40–48, https://doi.org/10.1016/j.jinorgbio.2018.10.012.

[12] W. Madden, E. Del Carpio, L. Hernández, L. Echevarria, V. Lubes, Mixed-ligand complexes of copper(II) with 1,10-phenanthroline and amino acids, Phys. Chem. Liq. 60 (2022) 786–807, https://doi.org/10.1080/00319104.2022.2053975.

[13] N.D. Corona-Motolinia, B. Martínez-Valencia, L. Noriega, B.L. Sánchez-Gaytán, A. Mendoza, F.J. Meléndez-Bustamante, M.E. Castro, E. González-Vergara, Ternary copper complex of L-glutamine and phenanthroline as counterions of cyclo-tetravanadate anion: experimental–theoretical characterization and potential antineoplastic activity, Metals 11 (2021), https://doi.org/10.3390/met11101541.

[14] S. Wang, Y. Zhao, Z. Zhang, Y. Zhang, L. Li, Recent advances in amino acid-metal coordinated nanomaterials for biomedical applications, Chinese J. Chem. Eng. 38 (2021) 30–42, https://doi.org/10.1016/j.cjche.2021.03.013.

[15] M.M.J. Smulders, I.A. Riddell, C. Browne, J.R. Nitschke, Building on architectural principles for three-dimensional metallosupramolecular construction, Chem. Soc. Rev. 42 (2013) 1728–1754, https://doi.org/10.1039/C2CS35254K.

[16] D. Romani, O. Noureddine, N. Issaoui, S.A. Brandán, Properties and reactivities of niclosamide in different media, a potential antiviral to treatment of COVID-19 by using DFT calculations and molecular docking, Biointerface Res. Appl. Chem. 10 (2020) 7295–7328, https://doi.org/10.33263/BRIAC106.72957328.

[17] F. Hammami, N. Issaoui, S. Nasr, Investigation of hydrogen bonded structure of urea-water mixtures through Infra-red spectroscopy and non-covalent interaction (NCI) theoretical approach, Comput. Theor. Chem. 1199 (2021) 113218, https://doi.org/10.1016/j.comptc.2021.113218.

[18] M. Medimagh, C. Ben Mleh, N. Issaoui, A.S. Kazachenko, T. Roisnel, O.M. Al-Dossary, H. Marouani, L.G. Bousiakoug, DFT and molecular docking study of the effect of a green solvent (water and DMSO) on the structure, MEP, and FMOs of the 1-ethylpiperazine-1,4-diium bis(hydrogenoxalate) compound, J. Mol. Liq. 369 (2023) 120851, https://doi.org/10.1016/j.molliq.2022.120851.

[19] A.S. Kazachenko, N. Issaoui, M. Medimagh, O. Yu Fetisova, Y.D. Berezhnaya, E. V Elsuf'ev, O.M. Al-Dossary, M.J. Wojcik, Z. Xiang, L.G. Bousiakou, Experimental and theoretical study of the sulfamic acid-urea deep eutectic solvent, J. Mol. Liq. 363 (2022) 119859, https://doi.org/10.1016/j.molliq.2022.119859.

[20] S. Gatfaoui, N. Issaoui, A. Mezni, F. Bardak, T. Roisnel, A. Atac, H. Marouani, Synthesis, structural and spectroscopic features, and investigation of bioactive nature of a novel organic-inorganic hybrid material 1H-1,2,4-triazole-4-ium trioxonitrate, J. Mol. Struct. 1150 (2017) 242–257, https://doi.org/10.1016/j.molstruc.2017.08.092.

[21] S. Medici, M. Peana, V.M. Nurchi, J.I. Lachowicz, G. Crisponi, M.A. Zoroddu, Noble metals in medicine: latest advances, Coord. Chem. Rev. 284 (2015) 329–350, https://doi.org/10.1016/j.ccr.2014.08.002.

[22] C. Hureau, P. Dorlet, Coordination of redox active metal ions to the amyloid precursor protein and to amyloid-β peptides involved in Alzheimer disease. Part 2: dependence of Cu(II) binding sites with Aβ sequences, Coord. Chem. Rev. 256 (2012) 2175–2187, https://doi.org/10.1016/j.ccr.2012.03.034.

[23] E. Gaggelli, H. Kozlowski, D. Valensin, G. Valensin, Copper homeostasis and neurodegenerative disorders (Alzheimer's, prion, and Parkinson's diseases and amyotrophic lateral sclerosis), Chem. Rev. 106 (2006) 1995–2044, https://doi.org/10.1021/cr040410w.

[24] F. Tisato, C. Marzano, M. Porchia, M. Pellei, C. Santini, Copper in diseases and treatments, and copper-based anticancer strategies, Med. Res. Rev. 30 (2010) 708–749, https://doi.org/10.1002/med.20174.

[25] D. Denoyer, S. Masaldan, L. Fontaine, M.A. Cater, Targeting copper in cancer therapy: 'Copper that Cancer', Metallomics 7 (2015) 1459–1476, https://doi.org/10.1039/C5MT00149H.

[26] A. Wojciechowska, J. Janczak, W. Zierkiewicz, P. Rytlewski, T. Rojek, M. Duczmal, Copper(II) complex with L-arginine – crystal structure, DFT calculations, spectroscopic, thermal and magnetic properties, Mater. Chem. Phys. 228 (2019) 272–284, https://doi.org/10.1016/j.matchemphys.2019.02.037.

[27] N. Zhang, J. Tang, Y. Ma, M. Liang, D. Zeng, G. Hefter, A spectroscopic study of solvent effects on the formation of Cu(II)–chloride complexes in aqueous solution, Phys. Chem. Chem. Phys. 23 (2021) 6807–6814, https://doi.org/10.1039/D0CP05243D.

[28] S. Kiraz, D. İnci, R. Aydın, Ö. Vatan, Y. Zorlu, T. Cavaş, Antiproliferative activity of copper(II) glutamine complexes with N,N-donor ligands: synthesis, characterization, potentiometric studies and DNA/BSA interactions, J. Mol. Struct. 1194 (2019) 245–255, https://doi.org/10.1016/j.molstruc.2019.05.086.

[29] B.H. Toby, EXPGUI, a graphical user interface for GSAS, J. Appl. Crystallogr. 34 (2001) 210–213, https://doi.org/10.1107/S0021889801002242.

[30] M.J. Frisch, G.W. Trucks, H.B. Schlegel, G.E. Scuseria, M.A. Robb, J.R. Cheeseman, G. Scalmani, V. Barone, G.A. Petersson, H. Nakatsuji, M.C. Li, A.V. Marenich, J. Bloino, B.G. Janesko, R. Gomperts, B. Mennucci, H.P. Hratchian, J.V. Ortiz, A.F. Izmaylov, J.L. Sonnenberg, D. Williams-Young, F.L.F. Ding, J.G.F. Egidi, B. Peng, A. Petrone, T. Henderson, D. Ranasinghe, V.G. Zakrzewski, J. Gao, N. Rega, G. Zheng, W. Liang, M. Hada, M. Ehara, K. Toyota, R. Fukuda, J. Hasegawa,

M. Ishida, T. Nakajima, Y. Honda, O. Kitao, H. Nakai, T. Vreven, K. Throssell, Jr. J.A.M, J.E. Peralta, F. Ogliaro, M.J. Bearpark, J.J. Heyd, E.N. Brothers, K. N. Kudin, V.N. Staroverov, T.A. Keith, R. Kobayashi, J. Normand, K. Raghavachari, A.P. Rendell, J.C. Burant, S.S. Iyengar, J. Tomasi, M. Cossi, J.M. Millam, M. Klene, C. Adamo, R. Cammi, J.W. Ochterski, R.L. Martin, K. Morokuma, O. Farkas, J.B. Foresman, D.J. Fox, Gaussian 16, 2016.
[31] C. Adamo, V. Barone, Toward reliable density functional methods without adjustable parameters: the PBE0 model, J. Chem. Phys. 110 (1999) 6158–6170, https://doi.org/10.1063/1.478522.
[32] J.G. de Oliveira Neto, J.R. Viana, A.L.A. Butarelli, A.P.A. dos Santos, M.R. Lage, A.O. dos Santos, Synthesis, physicochemical properties, and antitumor cytotoxic activity of the Mg(II) coordination complex containing 1,10-phenanthroline and sulfate ligands, Inorganica Chim. Acta. 556 (2023) 121658, https://doi.org/10.1016/j.ica.2023.121658.
[33] J.M.L. Martin, A. Sundermann, Correlation consistent valence basis sets for use with the Stuttgart–Dresden–Bonn relativistic effective core potentials: the atoms Ga–Kr and In–Xe, J. Chem. Phys. 114 (2001) 3408–3420, https://doi.org/10.1063/1.1337864.
[34] P. Schwerdtfeger, in: U. Kaldor, S. Wilson (Eds.), Relativistic Pseudopotentials BT - Theoretical Chemistry and Physics of Heavy and Superheavy Elements, Springer Netherlands, Dordrecht, 2003, pp. 399–438, https://doi.org/10.1007/978-94-017-0105-1_10.
[35] R. Cammi, J. Tomasi, Remarks on the use of the apparent surface charges (ASC) methods in solvation problems: iterative versus matrix-inversion procedures and the renormalization of the apparent charges, J. Comput. Chem. 16 (1995) 1449–1458, https://doi.org/10.1002/jcc.540161202.
[36] F. Teixeira, VibAnalysis: Tools for Performing Vibrational Analysis on Molecular Systems, 2017.
[37] F. Teixeira, M.N.D.S. Cordeiro, Improving vibrational mode interpretation using bayesian regression, J. Chem. Theor. Comput. 15 (2019) 456–470, https://doi.org/10.1021/acs.jctc.8b00439.
[38] J.P. Merrick, D. Moran, L. Radom, An evaluation of harmonic vibrational frequency scale factors, J. Phys. Chem. A 111 (2007) 11683–11700, https://doi.org/10.1021/jp073974n.
[39] A. Daina, O. Michielin, V. Zoete, SwissADME: a free web tool to evaluate pharmacokinetics, drug-likeness and medicinal chemistry friendliness of small molecules, Sci. Rep. 7 (2017) 42717, https://doi.org/10.1038/srep42717.
[40] F.L. Hirshfeld, Bonded-atom fragments for describing molecular charge densities, Theor. Chim. Acta 44 (1977) 129–138, https://doi.org/10.1007/BF00549096.
[41] M.A. Spackman, J.J. McKinnon, Fingerprinting intermolecular interactions in molecular crystals, CrystEngComm 4 (2002) 378–392, https://doi.org/10.1039/B203191B.
[42] J.J. McKinnon, M.A. Spackman, A.S. Mitchell, Novel tools for visualizing and exploring intermolecular interactions in molecular crystals, Acta Crystallogr. Sect. B Struct. Sci. 60 (2004) 627–668, https://doi.org/10.1107/S0108768104020300.
[43] P.R. Spackman, M.J. Turner, J.J. McKinnon, S.K. Wolff, D.J. Grimwood, D. Jayatilaka, M.A. Spackman, CrystalExplorer: a program for Hirshfeld surface analysis, visualization and quantitative analysis of molecular crystals, J. Appl. Crystallogr. 54 (2021) 1006–1011, https://doi.org/10.1107/S1600576721002910.
[44] J.J. McKinnon, D. Jayatilaka, M.A. Spackman, Towards quantitative analysis of intermolecular interactions with Hirshfeld surfaces, Chem. Commun. (2007) 3814–3816, https://doi.org/10.1039/B704980C.
[45] T. Mosmann, Rapid colorimetric assay for cellular growth and survival: application to proliferation and cytotoxicity assays, J. Immunol. Methods 65 (1983) 55–63. https://10.1016/0022-1759(83)90303-4.
[46] S. Adhikari, O. Hussain, R.M. Phillips, W. Kaminsky, M.R. Kollipara, Neutral and cationic half-sandwich arene d6 metal complexes containing pyridyl and pyrimidyl thiourea ligands with interesting bonding modes: synthesis, structural and anti- cancer studies, Appl. Organomet. Chem. 32 (2018) 1–13, https://doi.org/10.1002/aoc.4476.
[47] S.R. Liao, X.Y. Le, Q.B. Lin, Q.M. Lu, X.P. Liu, Y.H. Xiong, X.L. Feng, Experimental crystal structure determination of aqua-(L-glutamine-N,O)-(1,10-phenanthroline-N,N')-copper(II) chloride sesquihydrate, Chin. J. Inorg. Chem. 22 (2006) 201, https://doi.org/10.5517/cc94k54.
[48] A. Fathi Azarbayjani, N. Aliasgharlou, S. Khoshbakht, P. Ghanbarpour, E. Rahimpour, M. Barzegar-Jalali, A. Jouyban, Experimental solubility and density functional theory studies of deferasirox in binary solvent mixtures: performance of polarizable continuum model and Jouyban-Acree Model, J. Chem. Eng. Data 64 (2019) 2273–2279, https://doi.org/10.1021/acs.jced.8b01001.
[49] C.G. Zhan, J.A. Nichols, D.A. Dixon, Ionization potential, electron affinity, electronegativity, hardness, and electron excitation energy: molecular properties from density functional theory orbital energies, J. Phys. Chem. A 107 (2003) 4184–4195, https://doi.org/10.1021/jp0225774.
[50] J.A.O. Rodrigues, A.U. Torres, N.A.B. de Sousa, T.J.D. de Sousa, J.G. de Oliveira Neto, A.S. Reis, M.R. Lage, A.O. dos Santos, C.C. dos Santos, A.S. de Menezes, F. F. de Sousa, Synthesis, characterization, DFT study, and antibacterial activity of a coordination complex of Cu(II) with 1,10-phenanthroline and L-methionine ligands, J. Mol. Struct. 1293 (2023) 136197, https://doi.org/10.1016/j.molstruc.2023.136197.
[51] G. Zhang, C.B. Musgrave, Comparison of DFT methods for molecular orbital eigenvalue calculations, J. Phys. Chem. A 111 (2007) 1554–1561, https://doi.org/10.1021/jp061633o.
[52] C.G. Zhan, J.A. Nichols, D.A. Dixon, Ionization potential, electron affinity, electronegativity, hardness, and electron excitation energy: molecular properties from density functional theory orbital energies, J. Phys. Chem. A 107 (2003) 4184–4195, https://doi.org/10.1021/jp0225774.
[53] R.G. Parr, R.A. Donnelly, M. Levy, W.E. Palke, Electronegativity: the density functional viewpoint, J. Chem. Phys. 68 (1977) 3801–3807, https://doi.org/10.1063/1.436185.
[54] R.A. Costa, K.M.T. Oliveira, R.C.S. Nunomura, E.S.A. Junior, M.L.B. Pinheiro, E.V. Costa, A. Barison, Quantum chemical properties investigation and molecular docking analysis with DNA topoisomerase II of β-carboline indole alkaloids from Simaba guianensis: a combined experimental and theoretical DFT study, Struct. Chem. 29 (2018) 299–314, https://doi.org/10.1007/s11224-017-1029-5.
[55] R. Parthasarathi, V. Subramanian, D.R. Roy, P.K. Chattaraj, Electrophilicity index as a possible descriptor of biological activity, Bioorg. Med. Chem. 12 (2004) 5533–5543, https://doi.org/10.1016/j.bmc.2004.08.013.
[56] R.G. Parr, L.V. Szentpály, S. Liu, Electrophilicity index, J. Am. Chem. Soc. 121 (1999) 1922–1924, https://doi.org/10.1021/ja983494x.
[57] R.A.A. Ammar, A.N.M.A. Alaghaz, A.A. Elhenawy, DFT, characterization and investigation of vibrational spectroscopy of 4-(4-hydroxy)-3-(2-pyrazine-2-carbonyl)hydrazonomethylphenyl-diazen-yl- benzenesulfonamide and its copper(II) complex, J. Mol. Struct. 1067 (2014) 94–103, https://doi.org/10.1016/j.molstruc.2014.02.051.
[58] S. Kumar Richa, J. Sindhu, P. Choudhary, S. Jaglan, E. Zangrando, R. Kumar, S.C. Sahoo, V. Kumar, S.K. Mehta, R. Kataria, Exploration of synthesis, structural aspects, DFT studies and bio-efficacy of some new DHA-benzohydrazide based copper(II) complexes, J. Mol. Struct. 1228 (2021) 129460, https://doi.org/10.1016/j.molstruc.2020.129460.
[59] F.A. Mohammed, H.I. Abbood, Structural and electronic properties of cis-platin metal complex: B3LYP-SDD/DFT calculations, Int. J. Adv. Eng. Res. Sci. 4 (2017) 82–86, https://doi.org/10.22161/ijaers.4.7.12.
[60] S. Ghosh, Cisplatin: the first metal based anticancer drug, Bioorg. Chem. 88 (2019) 102925, https://doi.org/10.1016/j.bioorg.2019.102925.
[61] R. Mezencev, Interactions of cisplatin with non-DNA targets and their influence on anticancer activity and drug toxicity: the complex world of the platinum complex, Curr. Cancer Drug Targets 14 (2015) 794–816, https://doi.org/10.2174/1568009614666141128105146.
[62] I. Kostova, Platinum complexes as anticancer agents, Recent Pat, Anticancer. Drug Discov. 1 (2006) 1–22, https://doi.org/10.2174/157489206775246458.
[63] A. Nataraj, V. Balachandran, T. Karthick, Molecular orbital studies (hardness, chemical potential, electrophilicity, and first electron excitation), vibrational investigation and theoretical NBO analysis of 2-hydroxy-5-bromobenzaldehyde by density functional method, J. Mol. Struct. 1031 (2013) 221–233, https://doi.org/10.1016/j.molstruc.2012.09.047.
[64] M. Azam, S.I. Al-Resayes, A. Trzesowska-Kruszynska, R. Kruszynski, Synthesis, characterization and X-ray crystal structure of a mononuclear ampyrone based zinc complex, J. Mol. Struct. 1259 (2022) 132727, https://doi.org/10.1016/j.molstruc.2022.132727.
[65] S. Kansız, M. Azam, T. Basılı, S. Meral, F.A. Aktaş, S. Yeşilbağ, K. Min, A.A. Ağar, N. Dege, Synthesis, structural studies, Hirshfeld surface analysis, and molecular docking studies of a thiophene-based Schiff base compound, J. Mol. Struct. 1265 (2022) 133477, https://doi.org/10.1016/j.molstruc.2022.133477.
[66] S. Sundareswaran, S. Karuppannan, Hirshfeld surface analysis of stable and metastable polymorphs of vanillin, Cryst. Res. Technol. 55 (2020) 2000083, https://doi.org/10.1002/crat.202000083.

[67] B. Robert, E.B. Brown, Principles and Applications of Thermal Analysis, Blackwell Publishing Ltd, Oxford, UK, 2008, https://doi.org/10.1002/9780470697702.
[68] Y.C. Lien, W.W. Nawar, Thermal decomposition of some amino acids. Valine, Leucine and lsoleucine, J. Food Sci. 39 (1974) 911–913, https://doi.org/10.1111/j.1365-2621.1974.tb07274.x.
[69] I. Contineanu, A. Neacsu, S.T. Perisanu, The standard enthalpies of formation of l-asparagine and l-α-glutamine, Thermochim. Acta 497 (2010) 96–100, https://doi.org/10.1016/j.tca.2009.08.017.
[70] J.O. Carvalho, J.G. Oliveira Neto, J.G. Silva Filho, F.F. de Sousa, P.T.C. Freire, A.O. Santos, P.F. Façanha Filho, Physicochemical properties calculated using DFT method and changes of 5-methyluridine hemihydrate crystals at high temperatures, Spectrochim. Acta Part A Mol. Biomol. Spectrosc. 281 (2022) 121594, https://doi.org/10.1016/j.saa.2022.121594.
[71] K. Raznjevic, Tabele si diagrame termodinamice, Tehnica, Bucareste, 1978.
[72] D.L. Rousseau, R.P. Bauman, S.P.S. Porto, Normal mode determination in crystals, J. Raman Spectrosc. 10 (1981) 253–290, https://doi.org/10.1002/jrs.1250100152.
[73] L.F.L. Silva, W. Paschoal, G.S. Pinheiro, J.G. Da Silva Filho, P.T.C. Freire, F.F. De Sousa, S.G.C. Moreira, Understanding the effect of solvent polarity on the polymorphism of actadecanoic acid through spectroscopic techniques and DFT calculations, CrystEngComm 21 (2019) 297–309, https://doi.org/10.1039/c8ce01402g.
[74] D.C. Abreu, P.F.F. Filho, G.S. Pinheiro, P.T.C. Freire, S.G.C. Moreira, A.O. Dos Santos, F.F. De Sousa, Polymorphism at hexadecanoic-acid crystals investigated through structural and vibrational studies, Vib. Spectrosc. 121 (2022) 103402, https://doi.org/10.1016/j.vibspec.2022.103402.
[75] N.S. Santana, A.F. Gomes, H.S. Santana, G.D. Saraiva, P.R.S. Ribeiro, A.O. Santos, C.E.S. Nogueira, F.F. de Sousa, Phase transformations of azithromycin crystals investigated by thermal and spectroscopic analyses combined with *ab initio* calculations, Cryst. Growth Des. 21 (2021) 3602–3613, https://doi.org/10.1021/acs.cgd.1c00375.
[76] N. Rekik, N. Issaoui, H. Ghalla, B. Oujia, M.J. Wójcik, IR spectral density of H-bonds. Both intrinsic anharmonicity of the fast mode and the H-bond bridge. Part I: anharmonic coupling parameter and temperature effects, J. Mol. Struct. THEOCHEM 821 (2007) 9–21, https://doi.org/10.1016/j.theochem.2007.06.016.
[77] N. Mhadhbi, N. Issaoui, W.S. Hamadou, J.M. Alam, A.S. Elhadi, M. Adnan, H. Naïli, R. Badraoui, Physico-chemical properties, pharmacokinetics, molecular docking and in-vitro pharmacological study of a cobalt (II) complex based on 2-aminopyridine, ChemistrySelect 7 (2022) e202103592, https://doi.org/10.1002/slct.202103592.
[78] A.S. Kazachenko, Y.N. Malyar, N.Y. Vasilyeva, V.S. Borovkova, N. Issaoui, Optimization of guar gum galactomannan sulfation process with sulfamic acid, Biomass Convers. Biorefinery 13 (2023) 10041–10050, https://doi.org/10.1007/s13399-021-01895-y.
[79] J. Titiš, C. Rajnák, R. Boča, Energy levels in pentacoordinate d^5 to d^9 complexes, Inorganics 10 (2022) 116, https://doi.org/10.3390/inorganics10080116.
[80] M.A. Farrukh, Advanced Aspects of Spectroscopy, IntechOpen, 2012.
[81] J. Gao, S. Jiang, X. Zhang, Y. Fu, Z. Liu, Preparation, characterization and in vitro activity of a docetaxel–albumin conjugate, Bioorg. Chem. 83 (2019) 154–160, https://doi.org/10.1016/j.bioorg.2018.10.032.
[82] E.D. Harris, Cellular copper transport and metabolism, Annu. Rev. Nutr. 20 (2000) 291–310, https://doi.org/10.1146/annurev.nutr.20.1.291.
[83] C. Marzano, M. Pellei, F. Tisato, C. Santini, Copper complexes as anticancer agents, Anti Cancer Agents Med. Chem. 9 (2009) 185–211, https://doi.org/10.2174/187152009787313837.
[84] M. Ninomiya, K. Tanaka, Y. Tsuchida, Y. Muto, M. Koketsu, K. Watanabe, Increased bioavailability of tricin−amino acid derivatives via a prodrug approach, J. Med. Chem. 54 (2011) 1529–1536, https://doi.org/10.1021/jm1015457.
[85] L. Fang, M. Wang, S. Gou, X. Liu, H. Zhang, F. Cao, Combination of amino acid/dipeptide with nitric oxide donating oleanolic acid derivatives as PepT1 targeting antitumor prodrugs, J. Med. Chem. 57 (2014) 1116–1120, https://doi.org/10.1021/jm401634d.
[86] S. Zhang, Y. Zhu, C. Tu, H. Wei, Z. Yang, L. Lin, J. Ding, J. Zhang, Z. Guo, A novel cytotoxic ternary copper(II) complex of 1,10-phenanthroline and l-threonine with DNA nuclease activity, J. Inorg. Biochem. 98 (2004) 2099–2106, https://doi.org/10.1016/j.jinorgbio.2004.09.014.
[87] A.S. Boyer, D. Walter, C.S. Sørensen, DNA replication and cancer: from dysfunctional replication origin activities to therapeutic opportunities, Semin. Cancer Biol. 37–38 (2016) 16–25, https://doi.org/10.1016/j.semcancer.2016.01.001.
[88] D. Belkhir-Talbi, M. Makhloufi-Chebli, S. Terrachet-Bouaziz, D. Hikem-Oukacha, N. Ghemmit, L. Ismaili, A.M.S. Silva, M. Hamdi, Synthesis, characterization, theoretical studies, ADMET and drug-Likeness analysis: electrochemical and biological activities of metal complexes of 3-(2-hydroxybenzoyl)-2H-chromen-2-one, J. Mol. Struct. 1179 (2019) 495–505, https://doi.org/10.1016/j.molstruc.2018.11.035.
[89] P. Jain, V.K. Vishvakarma, P. Singh, S. Yadav, R. Kumar, S. Chandra, D. Kumar, N. Misra, Bioactive thiosemicarbazone coordination metal complexes: synthesis, characterization, theoretical analysis, biological activity, molecular docking and ADME analysis, Chem. Biodivers. 20 (2023) 1–11, https://doi.org/10.1002/cbdv.202300760.
[90] C.A. Lipinski, F. Lombardo, B.W. Dominy, P.J. Feeney, Experimental and computational approaches to estimate solubility and permeability in drug discovery and development settings, Adv. Drug Deliv. Rev. 64 (2012) 4–17, https://doi.org/10.1016/j.addr.2012.09.019.
[91] C.A. Lipinski, Lead- and drug-like compounds: the rule-of-five revolution, Drug Discov. Today Technol. 1 (2004) 337–341, https://doi.org/10.1016/j.ddtec.2004.11.007.